



THE UNIVERSITY *of* EDINBURGH

Edinburgh Research Explorer

Doppler Effect Assisted Wireless Communication for Interference Mitigation

Citation for published version:

Basnayaka, D & Ratnarajah, T 2019, 'Doppler Effect Assisted Wireless Communication for Interference Mitigation', *IEEE Transactions on Communications*. <https://doi.org/10.1109/TCOMM.2019.2912193>

Digital Object Identifier (DOI):

[10.1109/TCOMM.2019.2912193](https://doi.org/10.1109/TCOMM.2019.2912193)

Link:

[Link to publication record in Edinburgh Research Explorer](#)

Document Version:

Peer reviewed version

Published In:

IEEE Transactions on Communications

General rights

Copyright for the publications made accessible via the Edinburgh Research Explorer is retained by the author(s) and / or other copyright owners and it is a condition of accessing these publications that users recognise and abide by the legal requirements associated with these rights.

Take down policy

The University of Edinburgh has made every reasonable effort to ensure that Edinburgh Research Explorer content complies with UK legislation. If you believe that the public display of this file breaches copyright please contact openaccess@ed.ac.uk providing details, and we will remove access to the work immediately and investigate your claim.



Doppler Effect Assisted Wireless Communication for Interference Mitigation

Dushyantha A. Basnayaka¹, Senior Member, IEEE, and Tharmalingam Ratnarajah, Senior Member, IEEE

Abstract—Doppler effect is a fundamental phenomenon that appears in wave propagation, where a moving observer experiences dilation or contraction of the wavelength of a wave. It also appears in radio frequency (RF) wireless communication when there exists a relative movement between the transmitter and the receiver, and is widely considered as a major impairment for reliable wireless communication. The current paper proposes Doppler assisted wireless communication (DAWC) that exploits Doppler effect and uses kinetic energy for co-channel interference (CCI) mitigation. The proposed system also exploits the propagation environment and the network topology and consists of an access point (AP) with a rotating drum antenna. The rotating drum receive antenna is designed in such a way that it shifts the interfering signals away from the desired signal band. This paper includes a detailed system model, and the results show that under favorable fading conditions, CCI can be significantly reduced. Therefore, it is anticipated that more sophisticated wireless systems and networks can be designed by extending the basic ideas proposed herein.

Index Terms—Doppler effect, electromagnetic waves, co-channel interference, interference mitigation, kinetic energy.

I. INTRODUCTION

A MULTITUDE of wireless networks have revolutionized the modern living for a half a century, and are expected to revolutionize our lives in an unprecedented scale in the future too [1]. Today's wireless networks—often digital wireless networks—are used for various activities such as mass communication, security and surveillance systems, sensing and disaster monitoring networks, satellite communication and tactical communication systems. Wireless networks typically consist of a collection of wireless transmitters and receivers, and use a fixed band of radio frequency (RF) spectrum for communication. Due to spectrum scarcity, often wireless networks reuse their limited frequency spectrum, which in turn gives rise to a fundamental problem in wireless communication known as co-channel interference (CCI) [2].

The CCI occurs when wireless stations that are nearby use/reuse overlapping spectrum. Modern wireless networks widely employ many intelligent and adaptive physical (PHY)

layer interference mitigation/avoidance/management techniques such as interference detection and subtraction (also known as successive interference cancellation or SIC), coordinated multi-point systems (CoMP), interference alignment (IA), diversity receivers (such as maximal ratio combining (MRC), zero forcing (ZF) and minimum mean-squared error (MMSE)), cognitive radio (CR), cooperative communication and transmit power control. Often PHY layer techniques are more effective, but multiple access control (MAC) layer techniques such as schedule randomization, measurement and rescheduling, and super controller also exist [3]. Furthermore, cross layer techniques that combine and jointly optimize two or more MAC and PHY techniques for interference mitigation are also widely considered [4].

The PHY techniques add (or are expected to add) significant intelligence to future wireless networks. For instance, non-orthogonal multiple access systems (NOMA), which uses interference detection and subtraction along with power control is expected to increase the spectral efficiency and the system throughput in 5th generation (5G) mass communication networks [5], [6]. In CoMP, a number of co-channel transmitters provide coordinated transmission to multiple receivers and multiple receivers provide coordinated reception to multiple co-channel transmitters [7]. In IA, all the co-channel transmitters cooperatively align—by exploiting channel state information (CSI) at transmitters—their transmissions in such a way that the interference subspaces at all the receivers jointly are limited to a smaller dimensional subspace, and is orthogonal to the desired signal subspace [8]. Diversity receivers use multi-antenna techniques for interference mitigation [9], and CR learns from the environment, and adapts its transmission. If a particular channel is occupied by a primary user, CR halts transmission or transmits at a lower power level so that the possible interference to primary user is minimized [10].

The focus of this paper is also interference mitigation at PHY layer, where we envision to add a new degree of freedom to existing wireless receivers by exploiting Doppler effect. We introduce a new paradigm for wireless communication, namely Doppler Assisted Wireless Communication (DAWC in short) [11], and consider a receiver or an access point (AP) in a typical wireless sensor network with a circular high speed rotating drum antenna as shown in Fig. 1.

A. Rotating Drum Antenna

Fig. 1 illustrates the proposed circular drum antenna for DAWC. In order to exploit Doppler effect, the AP has a

Manuscript received July 16, 2018; revised December 19, 2018 and March 2, 2019; accepted April 6, 2019. This work was supported by the U.K. Engineering and Physical Sciences Research Council (EPSRC) under Grant EP/N014073/1. The associate editor coordinating the review of this paper and approving it for publication was A. Tajer. (Corresponding author: Dushyantha A. Basnayaka.)

The authors are with the Institute for Digital Communication, The University of Edinburgh, Edinburgh EH8 9YL, U.K. (e-mail: d.basnayaka@ed.ac.uk).

Color versions of one or more of the figures in this paper are available online at <http://ieeexplore.ieee.org>.

Digital Object Identifier 10.1109/TCOMM.2019.2912193

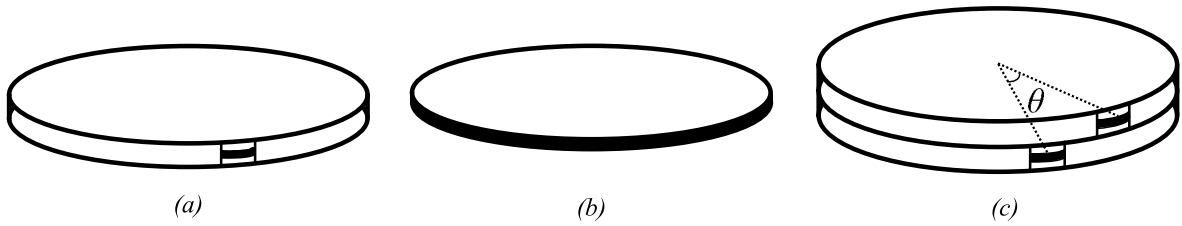


Fig. 1. A possible antenna implementation for Doppler assisted wireless communication (DAWC), where (a) a fixed antenna canister with an opening, where a small portion of the antenna is visible to outside, (b) a rotatable drum antenna, which is located inside the circular canister, (c) a possible implementation to receive two desired signals from two transmitters of azimuthal separation of θ .

86 circular antenna, which consists of two parts. 1) a fixed circular
 87 canister 2) a rotatable drum antenna as shown in Fig. 1-(b).
 88 The radiating surface of this conformal antenna lies on the
 89 curve surface of the drum, which is located inside the circular
 90 canister. There is an opening on the curve surface of the canis-
 91 ter, and it is directed to the direction of the desired transmitter.
 92 Consequently, the channel responses of the desired link and
 93 the other interfering links which have reasonable azimuthal
 94 separation exhibit different frequency characteristics. Despite
 95 Doppler effect being considered as a major impairment, the
 96 results in this paper indicate that successful receiver side CCI
 97 mitigation techniques (henceforth DAIM to denote Doppler
 98 assisted interference mitigation) can still be developed based
 99 on a rotating drum antenna and Doppler effect.

100 The round and/or rotating antenna units are used in several
 101 key widely-used systems such as TACAN (for tactical air
 102 navigation) and LIDAR (for light detection and ranging).
 103 The TACAN system has multiple antennas installed in a
 104 circle, and electronically steers a radio beam in order to
 105 provide directional information for distance targets over a
 106 360° azimuth. The radio beam rotates (often electronically)
 107 merely to serve targets located around it. However, the rotating
 108 antenna in DAWC is a key unit that gives rise to Doppler
 109 effect, and fundamentally important for the operation of
 110 the system. It typically rotates at very high speed than the
 111 beam in TACAN system. Furthermore, modern autonomous
 112 cars also employ a system known as LIDAR, which also
 113 has a rotating unit. LIDAR is a variation of conventional
 114 RADAR, and uses laser light instead of radiowaves to make
 115 high-resolution topological maps around automobiles. LIDAR
 116 antenna rotates in order merely to map 360° angle, and not
 117 for any other fundamental reason. The TACAN and LIDAR
 118 systems are hence fundamentally different from the system
 119 proposed in the current paper, and tackle entirely different
 120 challenges.

121 MIMO (or its more popular variant, massive MIMO) is
 122 the state-of-the-art for CCI mitigation, but heavily relies on
 123 CSI [12]. The proposed system does not rely on CSI for CCI
 124 mitigation (note however that, it still uses CSI of the desired
 125 user for data detection). Typically, CCI may occur from a
 126 single co-channel transmitter or numerous co-channel trans-
 127 mitters. If CCI occurs from multiple co-channel users, MIMO
 128 systems need fairly accurate CSI of all co-channel users for
 129 successful CCI mitigation [13]. They let the interference into
 130 the system, and uses ever more complex signal processing
 131 techniques (a software domain approach) for CCI mitigation.

In essence, massive MIMO lets the enemy (metaphorically
 to denote CCI) into its own backyard, and fight head-on.
 In contrast, the proposed system can handle any number of
 interferers, and automatically suppresses co-channel multi-
 path signals with a reasonable azimuthal separation to the
 desired multi-paths even before they corrupt the desired signal.
 In that sense, DAWC is a paradigm shifting technology, which
 keeps the enemy at the bay. Furthermore, the rotation is not a
 necessity. If CCI is not severe, and can be handled by software
 means, the antenna is not required to be rotated. The level of
 CCI mitigation can be controlled rapidly by simply changing
 the rotation speed of the antenna. In essence, DAWC adds a
 new degree of freedom to future wireless APs.

It is important to note furthermore that, the results in
 this paper are also applicable to wireless networks based on
 microwave, mmwave frequencies, and also to coherent optical
 laser communication systems [14], [15].

This paper includes a detailed study of DAWC on
 MATLAB. The rest of the paper also includes the system
 model in Sec. II, performance analysis and discussions in
 Sec. III, further remarks in Sec. IV, and conclusions in Sec. V.

II. SYSTEM MODEL

A narrow-band uplink communication from a wireless sta-
 tion, S (to denote source) to AP in a wireless network is
 considered, where another wireless station, I (to denote the
 interferer) located at an azimuthal angle separation of θ poses
 CCI as shown in Fig. 2. Note that, all wireless stations are
 fixed, and both S and I are in transmit mode while AP being
 in receive mode. It is assumed that AP has a rotating drum
 antenna of radius, R , with the canister opening being directed
 towards the desired transmitter, S . Let the analog complex
 baseband signal of the desired and the interfering stations
 respectively be given by $b_S(t)$ and $b_I(t)$:

$$b_S(t) = \Psi(a_S), \quad (1)$$

$$b_I(t) = \Psi(a_I), \quad (2)$$

where a_S and a_I respectively are the complex discrete time
 base-band data—drawn from a M -Quadrature Amplitude Mod-
 ulation (M -QAM) constellation, \mathcal{M} based on binary data
 signals, d_S and d_I —signals of stations, S and I and the
 operation $\Psi(\cdot)$ denotes the square root raised cosine (SRRC)
 pulse shaping operation [16]. Let the symbol time duration
 and the bandwidth of the data signals be denoted by T_s and
 B_w respectively, where typically $T_s = 1/B_w$. The transmit

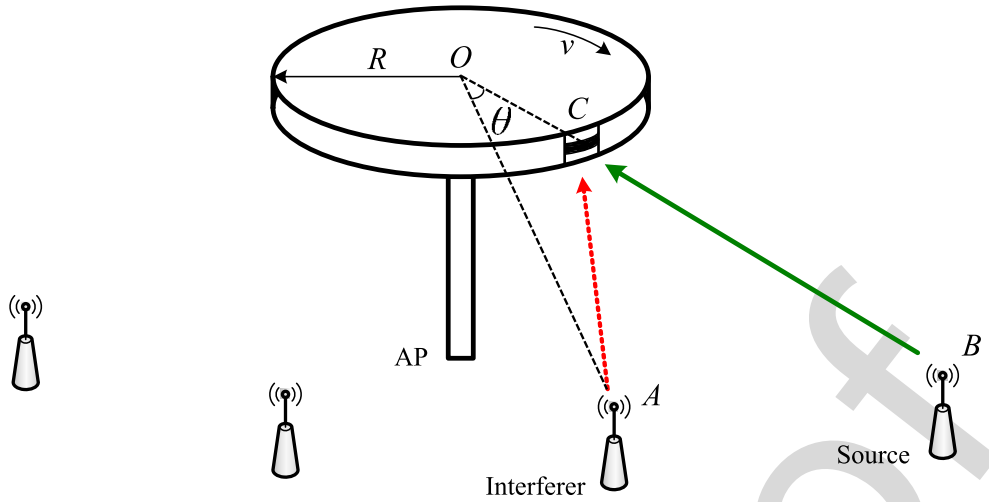


Fig. 2. A wireless AP with a single rotating antenna for DAWC. The figure is not to the scale, and the AP is exaggerated for exposition. To reduce the clutter, not all wireless links are shown.

175 waveforms will then be given by:

$$176 \quad x_S(t) = \text{Re} \{ b_S(t) e^{j2\pi f_c t} \}, \quad (3)$$

$$177 \quad x_I(t) = \text{Re} \{ b_I(t) e^{j2\pi f_c t} \}, \quad (4)$$

178 where f_c is the carrier frequency, $j = \sqrt{-1}$, and $\text{Re} \{ \}$ denotes
 179 the real part [17]. Furthermore, the transmit power of both
 180 links are scaled to give $\mathcal{E} \{ x_S(t)^2 \} = P_S$ and $\mathcal{E} \{ x_I(t)^2 \} =$
 181 P_I . It is herein assumed that the communication takes place
 182 between S , I and AP in a scattering environment, where AP
 183 receives multiple faded replicas of the transmitted signals,
 184 $x_S(t)$ and $x_I(t)$. Hence, the received signal by AP can in
 185 the absence of noise be given by:

$$186 \quad y(t) = \text{Re} \{ r_S(t) e^{j2\pi f_c t} \} + \text{Re} \{ r_I(t) e^{j2\pi f_c t} \}, \quad (5)$$

187 where the complex base-band desired and interfering received
 188 signals, $r_S(t)$ and $r_I(t)$ can be given by:

$$189 \quad r_S(t) = \sum_{n=0}^{N_S} \alpha_n^S e^{j\phi_n^S(t)} b_S(t - \tau_n^S), \quad (6a)$$

$$190 \quad r_I(t) = \sum_{n=0}^{N_I} \alpha_n^I e^{j\phi_n^I(t)} b_I(t - \tau_n^I). \quad (6b)$$

191 The quantities, α_n , ϕ_n and τ_n in (6) respectively are the faded
 192 amplitude, phase and path delay of the n th replica of the
 193 desired and interference signals, where:

$$194 \quad \phi_n^S(t) = 2\pi \{ f_n^S t - (f_c + f_n^S) \tau_n^S \}, \quad (7a)$$

$$195 \quad \phi_n^I(t) = 2\pi \{ f_n^I t - (f_c + f_n^I) \tau_n^I \}. \quad (7b)$$

196 It is assumed that α_n^S , α_n^I , τ_n^S , τ_n^I , N_S and N_I are approx-
 197 imately the same for a certain amount of time (say block
 198 interval) that is sufficient to transmit at least one data packet,
 199 and change to new realizations independently in the next block
 200 interval. The frequency change due to Doppler effect on the
 201 n th incoming ray of the desired and the interfering signal, f_n^S
 202 and f_n^I in (7) are respectively given by:

$$203 \quad f_n^S = f_m \sin(\beta_n^S), \quad (8a)$$

$$204 \quad f_n^I = f_m \sin(\theta + \beta_n^I), \quad (8b)$$

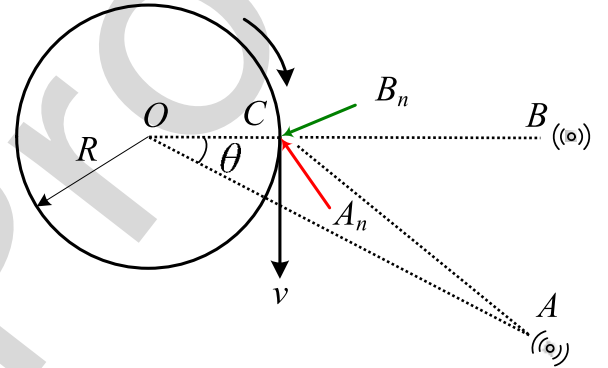


Fig. 3. The top view of an access point, where one desired (i.e. B_nC) and one interfering ray (i.e. A_nC) are shown. The canister opening is at C .

205 where $f_m = f_c v / C$. Note that the arrival angles of users
 206 are measured with respect to the direction of the respective
 207 user. For instance, the arrival angles, β_n^S of the desired
 208 user are measured with respect to the direction of CB (see
 209 Fig. 3), and the arrival angles, β_n^I of the interfering user
 210 are measured with respect to the direction of CA . As a result,
 211 according to Fig. 3, the n th angle of arrival of the desired
 212 and the interfering signals are given by $\beta_n^S = \angle BCB_n$ and
 213 $\beta_n^I = \angle ACA_n$. Furthermore, the dominant angles of arrivals
 214 are limited to $-\omega/2 \leq \beta_n^S, \beta_n^I \leq \omega/2$ for all n . Since
 215 it is a narrow-band communication link, we further assume
 216 that $\tau_n^S, \tau_n^I \ll T_s$, and with out loss of applicability, make
 217 the substitution, $\tau_S \approx \tau_n^S$ and $\tau_I \approx \tau_n^I$ for all n . As a
 218 result:

$$219 \quad r_S(t) = b_S(t - \tau_S) \sum_{n=0}^{N_S} \alpha_n^S e^{j\phi_n^S(t)}, \quad (9a)$$

$$220 \quad r_I(t) = b_I(t - \tau_I) \sum_{n=0}^{N_I} \alpha_n^I e^{j\phi_n^I(t)}, \quad (9b)$$

One must note that the approximations, $\tau_S \approx \tau_n^S$ and $\tau_I \approx \tau_n^I$ are invoked only to $b_S(t - \tau_n^S)$ and $b_I(t - \tau_n^I)$ in (9), and since, $f_c \tau_n^S$ and $f_c \tau_n^I$ can still be significant, the path delay differences are still considered in the summation of (9). If the perfect synchronization is assumed, the complex baseband desired and interfering received signals, $r_S(t)$ and $r_I(t)$ can be rewritten as:

$$r_S(t) = \left\{ \sum_{n=0}^{N_S} \alpha_n^S e^{j\phi_n^S(t)} \right\} b_S(t) = h_S(t) b_S(t), \quad (10a)$$

$$r_I(t) = \left\{ \sum_{n=0}^{N_I} \alpha_n^I e^{j\phi_n^I(t)} \right\} b_I(t) = h_I(t) b_I(t), \quad (10b)$$

where $h_S(t)$ and $h_I(t)$ are denoted henceforth as channel fading functions. The averaged channel gains for both links are defined as $\mathcal{E}\{|h_S(t)|^2\} = g_S$ and $\mathcal{E}\{|h_I(t)|^2\} = g_I$ [18]. The constants, g_S and g_I capture the average channel gains due to path loss and shadowing alone which is also given by $g_S = \mathcal{E}\left\{\sum_{n=0}^{N_S} (\alpha_n^S)^2\right\}$ and $g_I = \mathcal{E}\left\{\sum_{n=0}^{N_I} (\alpha_n^I)^2\right\}$, where the expectation is over block intervals.

It is assumed that dominant (in terms of the receive power) paths exist from both source and interferer to AP either as a result of line-of-sight (LoS) or dominant non-line-of-sight (NLoS) rays along with significantly weaker scattered rays. With out loss of generality, let the 0th terms in (6) denote the dominant paths, and as also pointed out earlier, AP points the canister opening towards dominant paths from S . Let K be Rician K -factor which models the ratio of the received power between the dominant path and other paths [16]. Then:

$$K = \frac{\mathcal{E}\left\{(\alpha_0^S)^2\right\}}{\mathcal{E}\left\{\sum_{n=1}^{N_S} (\alpha_n^S)^2\right\}} = \frac{\mathcal{E}\left\{(\alpha_0^I)^2\right\}}{\mathcal{E}\left\{\sum_{n=0}^{N_I} (\alpha_n^I)^2\right\}}, \quad (11)$$

where it is assumed that K -factor is the same for both the desired and interference link. The received signal in the presence of noise is given by:

$$y(t) = \text{Re}\left\{[r_S(t) + r_I(t) + n(t)]e^{j2\pi f_c t}\right\}, \quad (12)$$

where $n(t)$ is complex base-band zero mean additive white Gaussian noise (AWGN) signal with $\mathcal{E}\{|n(t)|^2\} = \sigma_n^2$. The signal-to-noise-ratio is hence defined as $\text{SNR} = g_S P_S / \sigma_n^2$, and signal-to-interference power ratio is defined as $\text{SIR} = g_S P_S / g_I P_I$. The AP processes the received signal, $y(t)$ by in-phase and quadrature-phase mixing and filtering with a low pass filter (LPF) of bandwidth, B_w to obtain the continuous-time complex base-band equivalent received signal as:

$$r(t) = r'_S(t) + r'_I(t) + n(t). \quad (13)$$

One must distinguish the difference between $r_S(t)$ and $r'_S(t)$ (also between $r_I(t)$ and $r'_I(t)$) in (13) that $r'_S(t)$ is the low pass filtered version of $r_S(t)$ which is the original faded desired signal supposed to be received by AP. Conventionally, LPF assures that $r'_S(t) = r_S(t)$ and $r'_I(t) = r_I(t)$. However as v increases, and also discussed in detail in Sec. II-A, $r_S(t)$ and $r_I(t)$ broaden in the frequency domain due to Doppler effect. Since the canister is directed towards the

desired source, the spectral broadening in $r_S(t)$ is less severe, and under favorable fading conditions, reliable communication is still possible with a reasonable channel estimation overhead. Moreover, if v is sufficiently large, the spectrum of $r_I(t)$ shifts to an intermediate frequency determined by v and θ . Consequently, a majority or entire interference signal, $r_I(t)$, can be made to be filtered out by LPF so to create a less interfered channel. The AP samples $r(t)$ at symbol rate to obtain the discrete time complex base-band signal in terms of desired data signal, a_S as:

$$r(\ell) = r'_S(\ell) + n'(\ell), \quad (14a)$$

$$= h'_S(\ell) a_S(\ell) + n'(\ell), \quad \forall \ell \quad (14b)$$

where ℓ alone is used for ℓT_s . Furthermore, $r'_S(\ell)$ and $n'(\ell)$ are the sampled versions of $r'_S(t)$ and $r'_I(t) + n(t)$ respectively. Note that $h'_S(\ell)$ combines the effect of $h_S(\ell)$ and other possible effects of low pass filtering of $r_S(\ell)$. The detector then uses the following symbol-by-symbol detection rule based on minimum Euclidean distance (also equivalent to maximum likelihood (ML) detector in AWGN) which treats the interference plus noise, $n'(\ell)$, as additional noise to obtain the estimated data, \hat{d}_S :

$$\hat{d}_S(\ell) = \min_{a_S(\ell) \in \mathcal{M}} |r(\ell) - h'_S(\ell) a_S(\ell)|^2, \quad \forall \ell. \quad (15)$$

Unlike in the case with $v = 0$, due to Doppler effect, $h'_S(\ell)$ are different within a block interval even with $\alpha_n, \phi_n, \tau_n, N_S$ and N_I being fixed. However, in this study, we assume that they can be approximated by a fixed value, \hat{h}_S . Consequently, (15) becomes:

$$\hat{d}_S(\ell) = \min_{a_S(\ell) \in \mathcal{M}} |r(\ell) - \hat{h}_S a_S(\ell)|^2, \quad \forall \ell. \quad (16)$$

where \hat{h}_S is the estimated value of h_S . The key roles played by spectral characteristics of channel fading functions in (10) are graphically discussed in the next section.

A. The Effects of Antenna Rotation

Conventionally, the antenna is fixed (i.e. $v = 0$), but as rotation speed increases, two conflicting phenomena happen. These phenomena can be better explained using the illustrations in Fig. 4. The Fig. 4-(a) shows an illustration of the single-sided magnitude response of $r_S(t)$, $r_I(t)$, $h_S(t)$ and $h_I(t)$ along with the magnitude response of the receiver's LPF. When $v = 0$, $H_S(f)$ and $H_I(f)$ are just impulses, and have no relevant effect on $r_S(f)$ and $r_I(f)$. However, as v increases $H_S(f)$ and $H_I(f)$ tend to broaden, and notably, $H_I(f)$ sways away from zero frequency (i.e., $f = 0$) to an intermediate frequency determined by $f_D = f_m \sin \theta$, and in turn by the azimuthal separation, θ , v , and f_c . Consequently, the majority of interference power lies outside the desired signal bandwidth, B_w , and hence, there is an interference suppression effect. On the other hand, since, $R_S(f) = H_S(f) \otimes B_S(f)$ and $R_I(f) = H_I(f) \otimes B_I(f)$, $R_S(f)$ and $R_I(f)$ also tend to broaden. Note that $B_S(f)$ and $B_I(f)$ denote the frequency response of $b_S(t)$ and $b_I(t)$ respectively, and \otimes denotes the convolution operator [16]. As a result of

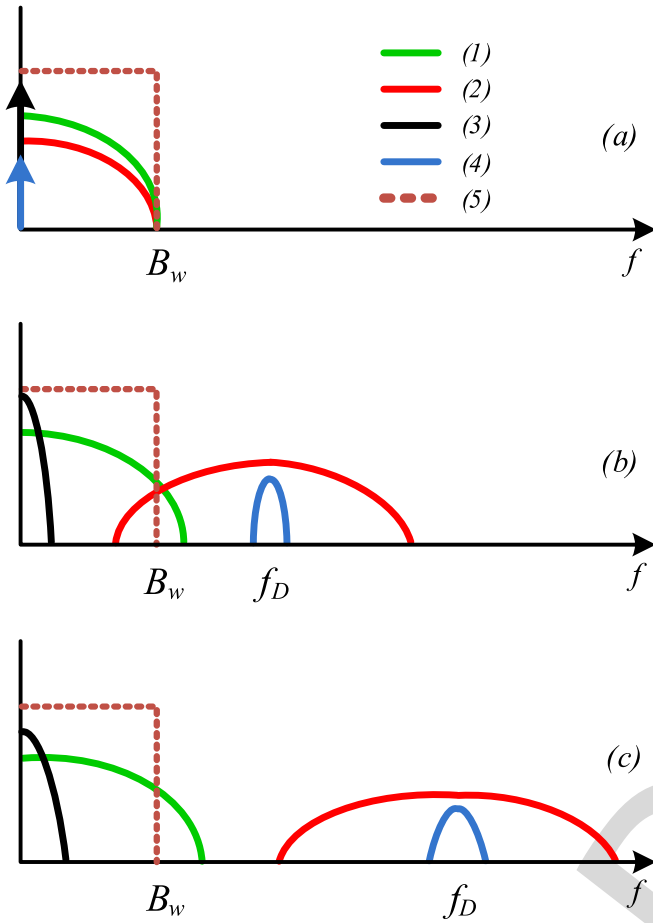


Fig. 4. Illustrations of magnitude responses of (1) $R_S(f)$, (2) $R_I(f)$, (3) $H_S(f)$ and (4) $H_I(f)$ which are Fourier transforms of $r_S(t)$, $r_I(t)$, $h_S(t)$ and $h_I(t)$ respectively. The magnitude response of LPF at AP is also shown in (5), and $f_D = \frac{v}{c} f_c \sin \theta$.

320 this spectrum broadening,¹ a certain amount of desired signal power is also suppressed by LPF and thus a distortion effect on the desired signal. As v increases further, as shown in 321 Fig. 4-(c), the interference signal can be shifted completely 322 away from the desired signal, but the amount of power suppressed by the LPF also increases making the desired 323 signal more distorted. Hence, a trade off between interference 324 suppression capability and the distortion of the desired signal 325 in DAWC is clearly apparent. However, as shown in Sec. III-F, 326 a reasonable compromise can be made, where a significant 327 performance gain can still be achieved. 328 329 330

331 III. PERFORMANCE ANALYSIS AND DISCUSSION

332 The performance of DAIM (a convenient name for DAWC 333 when applied for CCI mitigation) is analyzed using a compre- 334 hensive end-to-end digital communication link simulated on 335 MATLAB. In order to accurately assess DAIM, we herein 336 simulate a pass-band digital communication link, where 337 pulse shaping, up-conversion, RF mixing and LPF have also

¹The spectral broadening is initiated by the rotation, but could be exacerbated by adverse fading conditions such as low K , and high N_S , N_I and ω .

TABLE I
NOTATIONS AND THEIR DEFINITIONS

Definition	Symbol
Carrier frequency	f_c
Speed of light	C
Sampling frequency	F_s
Signal bandwidth	B_w
Symbol duration	T_s
Rician factor	K
Number of S/I multi-path components	N_S/N_I
Amplitude of the n th S/I multi-path	α_n^S/α_n^I
Phase of the n th S/I multi-path	ϕ_n^S/ϕ_n^I
Delay of the n th S/I multi-path	τ_n^S/τ_n^I
Azimuthal separation of S and I	θ

338 been implemented.² The main block diagram of the simulation 339 is shown in Fig. 5, where for simplicity Quadrature Phase Shift 340 Keying (QPSK) is considered with other system parameters as 341 shown in Tables I and II. The major steps of the simulation 342 environment are obtained as follows.

343 A. Transmit Signals

344 We consider a time duration to transmit a single data packet, 345 where a single packet lasts L symbols or equivalently ηL 346 samples. The constant, η denotes the up-sampling ratio, which 347 is given by $\eta = T_s/t_o$, where $t_o = 1/F_s$ is the sampling 348 period in the computer simulation herein. The k th sample of 349 the complex base-band transmitted signal of the desired link³ 350 is obtained by:

$$b_S(kt_o) = [\tilde{a}_S \otimes p](kt_o), \quad k = 1, \dots, \eta L, \quad (17)$$

351 where \tilde{a}_S is the k th sample of up-sampled version of a_S and 352 $p(kt_o)$ is the k th sample of SRRC filter which is obtained 353 by: 354

$$p(kt_o) = \frac{\sin(\pi k(1-\rho)) + 4\pi k \cos(\pi k(1+\rho))}{\pi k(1-16k^2\rho^2)}, \quad (18)$$

355 where ρ is the roll-off factor of SRRC filter. Henceforth, 356 we may interchangeably use standalone k for kt_o . Fur- 357 thermore, we scale $b_S(kt_o)$ so $\mathcal{E}\{|x_S(k)|^2\} = P_s/\eta =$ 358 $1/\eta$. Consequently, the k th sample of the normalized com- 359 plex base-band faded desired received signal⁴ is obtained 360 by: 361

$$r_S(k) = b_S(k) h_S(k). \quad (19)$$

²Note that the implementation of up-conversion and RF mixing which requires a significantly higher sampling rate, and hence is computationally inefficient, is avoided by using an equivalent base-band model, but still with transmit pulse shaping and LPF in order to accurately captures the effects outlined in Sec. II-A. Unlike in conventional complex base-band simulations, the LPF operation is crucial for this simulation study.

³Note that one can obtain the k th sample of the pass-band transmit signal of the desired link by $x_S(kt_o) = b_S(kt_o) e^{j2\pi f_c kt_o}$.

⁴Note that one can obtain the k th sample of the complex pass-band desired received signal by $\text{Re}\{r_S(k) e^{j2\pi f_c k}\}$.

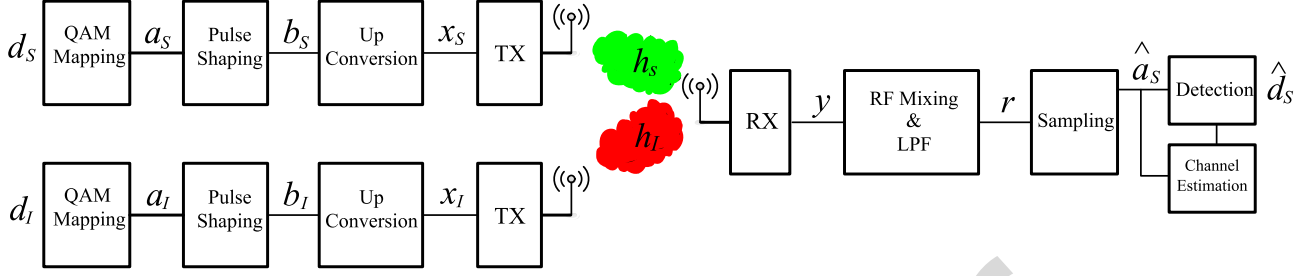


Fig. 5. The main simulation block diagram.

B. Multi-Path Channels

The k th sample of the fading function, $h_S(k)$ is obtained by the complex equation:

$$h_S(k) = \sqrt{\frac{g_S K}{K+1}} [h_S]_d + \sqrt{\frac{g_S}{K+1}} [h_S]_s, \quad (20)$$

where the channel function of the direct path of the desired link, $[h_S]_d = e^{-j\varphi_0^S}$, and the channel function of the scattered paths, $[h_S]_s$ is obtained as:

$$[h_S]_s = \sum_{n=1}^{N_S} \alpha_n^S e^{j2\pi f_n^S k t_o - j\psi_n^S}. \quad (21)$$

The term that accounts for the change in the frequency due to Doppler effect, f_n^S is obtained by $f_n^S = f_m \sin(\beta_n^S)$, where $\beta_n^S \sim \mathcal{U}(-\omega/2, \omega/2)$. Note that $\mathcal{U}(a, b)$ is an abbreviation for the uniform distribution with support, $[a, b]$. The phase term, ψ_n^S is obtained by $\psi_n^S \sim \mathcal{U}(0, 2\pi)$. More importantly, note that $f_0^S = 0$ for any v due to the fact that canister opening is directed towards to the desired transmitter. Furthermore, in LoS fading, ψ_0^S is dependent on the distance between S and AP, and hence is set to a fixed arbitrary value throughout the simulation. Lastly, the amplitudes, α_n^S are assumed to be approximately equal, and hence, are set to $\alpha_n^S = \sqrt{1/2N_S}$ which in conjunction with (20) subsequently guarantees that $\mathcal{E}\{|h_S(k)|^2\} = g_S$. This along with the fact that $\mathcal{E}\{|x_S(k)|^2\} = 1/\eta$ directly implies that $\mathcal{E}\{|r_S(k)|^2\} = 1/\eta$. Similarly, the k th sample of the scattered received signal of the interfering link, $r_I(k t_o)$ is also obtained with following notable exceptions: $[h_S]_d = e^{j2\pi f_0^I - j\psi_0^I}$, where $f_0^I = f_m \sin \theta$. Furthermore, β_n^I and ψ_n^I are assumed to be distributed as in the case for the desired link.

C. Receive Signal at AP

As a result, the k th sample of the combined pass-band received signal by AP is obtained as:

$$y(k) = \text{Re}\{[r_S(k) + r_I(k) + n(k)] e^{j2\pi f_c k}\}, \quad (22)$$

where $n(k)$ is the k th AWGN sample with variance σ_n^2/η , and since $r_S(k)$ and $r_I(k)$ are normalized to have average channel gains, g_S and g_I respectively, SIR of the wireless network boils down to $\text{SIR} = g_S/g_I$, and can be adjusted conveniently by manipulating, g_S and g_I in the computer simulation herein. Furthermore, SNR also boils down to $\text{SNR} = g_S/\sigma_n^2$.

D. RF Mixing, LP Filtering, Sampling and Detection

It is assumed herein that AP performs I/Q mixing perfectly,⁵ and produces a base-band version of $y(k)$, which is $r_S(k) + r_I(k) + n(k)$. The AP then passes this complex base-band version of $y(k)$ through SRRRC LPF. The low pass filtered complex signal is then sampled (rather down-sampled) at symbol rate of T_s to obtain $r(\ell T_s)$, for $\ell = 1, \dots, L$, which are the faded, interfered and noisier versions of the complex modulated samples, $a_S(\ell T_s)$, $\forall \ell$. The L complex samples per packet are then forwarded to the detector in (16) to obtain the reproduced data, \hat{d}_S .

E. Simple Channel Estimation

As pointed out in Sec. II, despite being different, all fading coefficients, $h'_S(\ell)$ s, in a single data packet duration are approximated by a single value, \hat{h}_S . In this study, we assume that the desired transmitter sends Q number of known data symbols, and AP uses simple least-square (LS) algorithm for channel estimation [19]. From (14), the complex base-band signal received in the channel estimation phase, $r^e(\ell)$, is:

$$r^e(\ell) = h'_S(\ell) a_S^e(\ell) + n'(\ell), \quad \text{for } \ell = 1, \dots, Q, \quad (23)$$

$$\approx \hat{h}_S a_S^e(\ell) + n'(\ell), \quad (24)$$

where $a_S^e(\ell)$ are known symbols transmitted for channel estimation. The LS estimation of \hat{h}_S can hence be obtained as: $\hat{h}_S = (\mathbf{a}_S^e)^H \mathbf{r}^e / (\mathbf{a}_S^e)^H \mathbf{a}_S^e$, where $\mathbf{r}^e = \{r^e(1), \dots, r^e(Q)\}^T$ and $\mathbf{a}^e = \{a_S^e(1), \dots, a_S^e(Q)\}^T$. In the forthcoming simulation study, $Q = 8$ is used.

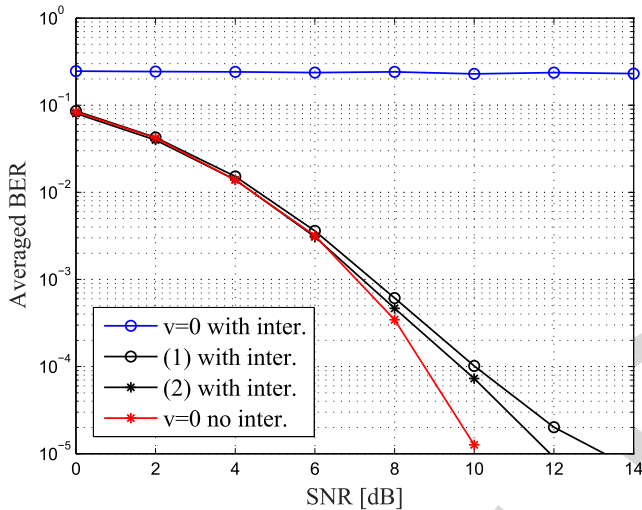
F. Simulation Results

A severely interfered link is simulated, where both desired and interference links have equal average link gains, so $g_I = g_S$. Hence, the SIR before the DAIM receiver denoted herein as SIR is 0 dB. Fig. 6 shows the averaged BER performance of a communication link with SIR = 0 dB, $N_S = N_I = 50$, $K = 20$ dB, and $\omega = 20^\circ$, where the results show that when $v = 0$, the link with interference is completely unusable. However, as v increases to $v = 2.5\lambda_c B_w$, BER performance improves significantly. BER performance with no interference and $v = 0$ is also shown for comparison. It is apparent that at low SNR, DAIM can create an interference free link, but

⁵Note that one can obtain the k th sample of the in-phase mixed signal by $y(k) \cos 2\pi f_c k$ while $y(k) \sin 2\pi f_c k$ being the quadrature phase mixed signal.

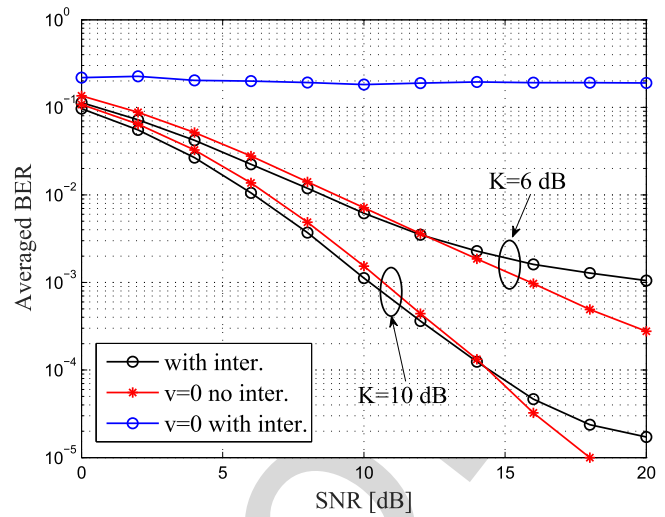
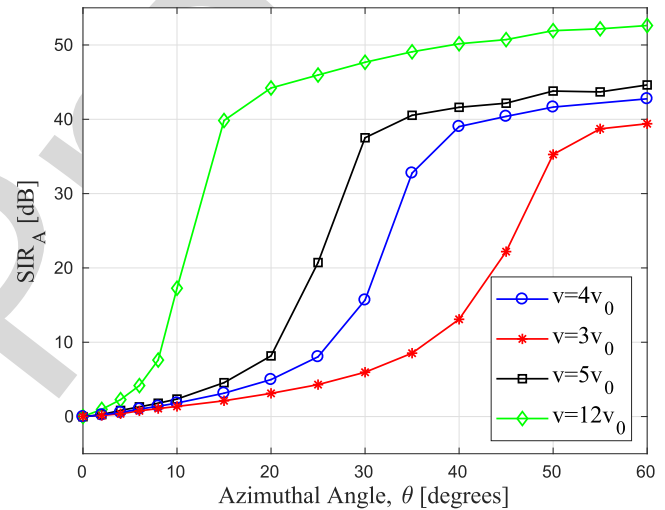
TABLE II
 PARAMETERS FOR QPSK PASS-BAND SIMULATION

Parameter	Value
Carrier frequency, f_c	60 GHz
Sampling frequency, F_s	3 MHz
Signal bandwidth, B_w	5 KHz
Symbol duration, T_s	$1/B_w$
Low pass filter	SRRC
SRRC span	$64T_s$
Rolloff factor of SRRC, ρ	0.2
Over sampling rate, η ,	300
Packet Length, L	$500T_s$


 Fig. 6. BER performance of DAIM, where SIR = 0 dB, $K = 20$ dB, $N = 50$, $\omega = 20^\circ$, and v is set such that in (1), $f_D = 10.8$ KHz and in (2), $f_D = 12.9$ KHz.

438 as SNR increases, BER performance drifts away. This trend
 439 can be attributed to the phenomenon that as v increases, the
 440 spectrum of the desired signal $h_S(t)b_S(t)$ broadens, which
 441 in turn makes a certain amount of desired signal power
 442 suppressed by LPF at AP.

443 Fig. 7 shows BER performance of the proposed interference
 444 mitigation system with SIR = 0 dB, $N = 20$, $K = 6/10$ dB
 445 and $\omega = 10^\circ$. As v increases, similar to Fig. 6, BER
 446 performance significantly improves specially at low SNR.
 447 As SNR increases BER performance again drifts away from
 448 BER performance of the completely interference free link.
 449 In this fading condition, two major factors come into effect.
 450 The first one is the effect that in low K values, the spectral
 451 broadening of $h_S(t)$ is severe, and hence a relatively larger
 452 amount of power is suppressed by LPF. The second one is
 453 the channel estimation errors. In the absence of significantly
 454 dominant multi-path components, the volatility of $h_S(t)$ even
 455 in the time duration of a single packet may be considerable.
 456 Approximating $h_S(\ell)$ for all ℓ s by a single \bar{h}_S is obviously
 457 suboptimal, and hence, more tailored algorithms for desired
 458 channel estimation may be needed. Furthermore, it is anti-
 459 cipated that more scenario specific low pass filters that passes
 460 a majority of desired signal power will be more effective for
 461 the earlier challenge as well.


 Fig. 7. BER performance of DAIM, where SIR = 0 dB, $K = 6/10$ dB, $N = 20$, $\omega = 10^\circ$ degrees, and v , when rotating, is set such that $f_D = 17.3$ KHz.

 Fig. 8. SIR_A performance of DAIM for SIR = 0 dB, where $K = 10$ dB, $N = 20$, and $\omega = 10^\circ$. Note that $v_0 = \lambda_c B_w$.

462 Fig. 7 also shows that BER of DAIM is marginally better
 463 than BER of interference free link with $v = 0$. This gain,
 464 though small, is defined as *Doppler Gain (DG)*. Doppler effect
 465 causes the fading function, $h_S(t)$, to fluctuate specially in low
 466 K and high N_S and ω . As a result, certain fading coefficients,
 467 $h_S(\ell)$, enhance their respective data symbols. Consequently,
 468 a net BER gain, which is manifested in the BER performance
 469 as DG, can be achieved. The simulation results that do not
 470 appear in this paper for reasons of space also show that
 471 ideal channel state information of the desired link significantly
 472 increases both BER of DAIM and DG.

473 Fig. 8 shows another view point of CCI mitigation capability
 474 of DAWC. Let the SIR after DAIM be denoted by SIR_A ,
 475 and:

$$476 \quad SIR_A = \frac{\mathcal{E}\{|r'_S(t)|^2\}}{\mathcal{E}\{|r'_I(t)|^2\}}, \quad (25)$$

477 where $r'_S(t)$ and $r'_I(t)$ are given in (13). Fig. 8 shows the
 478 SIR_A performance of DAIM against the azimuthal separation,
 479 θ for different rotation speeds. It can be seen here that higher

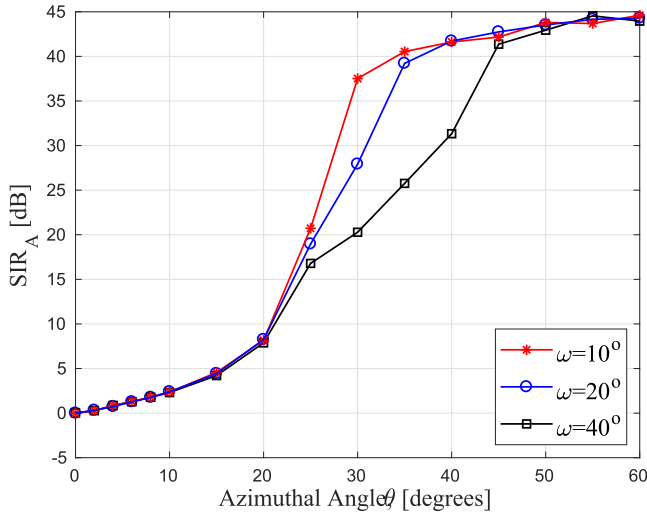


Fig. 9. SIR_A performance of DAIM for $SIR = 0$ dB, where $K = 10$ dB, $N = 20$, and $\omega = 10^\circ/20^\circ/40^\circ$. Note that $v = 5v_0$.

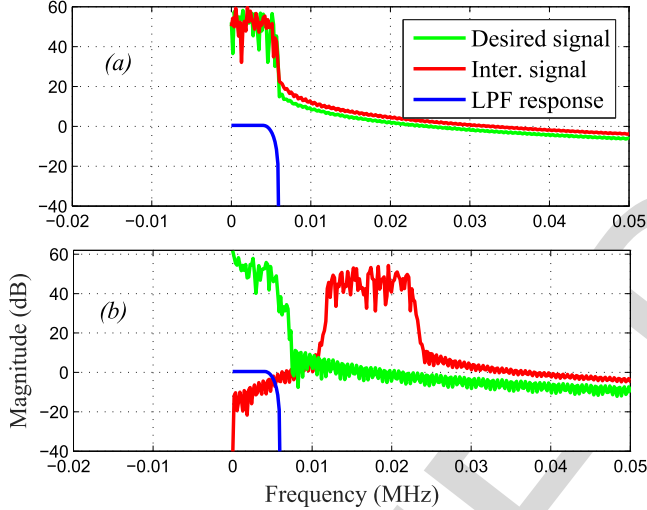


Fig. 10. Spectral characteristics of faded signals, $h_S(t)b_S(t)$ and $h_I(t)b_I(t)$, where $SIR = 0$ dB, $K = 10$ dB, $N = 20$, $\omega = 10^\circ$ degrees. In (a) $v = 0$ and in (b), v is set such that $f_D = 17.3$ KHz.

rotation speed may be required to achieve a certain SIR_A for low θ s and vice versa. Furthermore, Fig. 9 shows SIR_A performance of DAIM for various angle spreads ($\omega = 10^\circ/20^\circ/40^\circ$) for a fixed rotation speed of $v = 5v_0$, where $v_0 = \lambda_c B_w$.

Fig. 10-(a) and (b) show the spectral characteristics of faded signals, $h_S(t)b_S(t)$ and $h_I(t)b_I(t)$ with static and rotating antenna respectively. Herein, we consider a fading scenario, where $SIR = 0$ dB, $K = 10$ dB, $N = 20$, $\omega = 10^\circ$ degrees, and v is set, when rotating, such that $f_D = 17.3$ KHz. The figure clearly shows that as v increases, the interference signal, $h_I(t)b_I(t)$ shifts to an intermediate frequency so that it is suppressed by LPF. Furthermore, the spectral broadening, as v increases, of the desired signal is also visible in Fig. 10.

G. Important Remarks

As shown in Sec. III-F, DAIM suppresses CCI significantly as v increases. The optimum v is dependent on many system parameters such as B_w , f_c and environmental and topological parameters such as θ , ω , and K . Hence, v should be carefully selected, and be able to be adapted to the environment. From

Fig. 6 and also in general, a rotation velocity that achieves $f_D = 2B_w$ (which is about $v = 2\lambda_c B_w \sin \theta$) is a reasonable value for v . It is equivalent to $v = 58$ m/s for $B_w = 5$ KHz, and $v = 23$ m/s for $B_w = 2$ KHz. From geometry of the drum antenna, the angular rotation speed can be obtained as:

$$s_r = \frac{30v}{\pi R} = \frac{60CB_w}{\pi f_c R} \text{ RPM}, \quad (26)$$

where s_r is the angular rotation speed in rounds per minute (RPM), which is about 1100 RPM for $B_w = 2$ KHz, $R = 20$ cm and $f_c = 60$ GHz. The equation, (26) also shows that R and s_r can be traded-off for one another. Furthermore, it appears that DAIM can only be applied practically for mmWave frequencies with B_w in the order of KHz and ultra-narrowband (UNB) communication systems with sub-GHz carrier frequencies with B_w in the order of Hz. Other scenarios may require extremely high rotation velocities which may not be practically realizable with today's technologies. Otherwise, the results presented in this paper theoretically hold for any system that satisfies the assumptions considered in this paper.

In wireless communication, all the multi-path signals contribute to the receive signal power. As rotation speed increases some desired multi-path signals that give rise to excessive Doppler shift could also (while, of course, suppressing majority of interfering multi-path signals) be suppressed out by the low pass filter (See Fig. 4-(b) and (c)). It is important to note herein that, in the proper and advanced design of DAWC systems, the choice of the rotating speed should strike an effective balance between suppressing the interfering multi-paths and the desired multi-paths.

IV. FURTHER REMARKS

A. Multi-Antenna Configurations

The DAWC systems can also be extended to accommodate multiple antennas and users as shown in Fig. 11, where a possible configuration for multi-antenna Doppler assisted system for single-user communication is shown in Fig. 11-(a). Extending (13) to a dual-antenna configuration (merely for simplicity, but readily extends to more than two antenna cases) give rise to following base-band analogue equations:

$$r_1(t) = r'_{S1}(t) + n'_1(t), \quad (27a)$$

$$r_2(t) = r'_{S2}(t) + n'_2(t). \quad (27b)$$

Note that (27) applies after low-pass filtering, and hence $r'_{S_i}(t) = h'_{S_i}(t)b_S(t)$ for $i = 1, 2$. Note herein that $h'_{S_i}(t) \neq h_{S_i}(t)$ due to Doppler effect and subsequent low-pass filtering. As shown in Fig. 12, the canisters are stacked vertically, and hence both elevation and the azimuth of the incoming rays are considered in this simulation. Consequently,⁶

$$h_{S_i}(t) = \sum_{n=0}^{N_S} \alpha_n^S e^{j2\pi f_n^S t - j\psi_n^S + j(i-1)d \cos \phi_n^S}, \quad (28)$$

⁶It is assumed herein that unit wave vector of the n th desired wave front is given by $\sin \phi_n^S \sin \beta_n^S \mathbf{i} + \sin \phi_n^S \cos \beta_n^S \mathbf{j} + \cos \phi_n^S \mathbf{k}$, and antenna velocity vector of the i th drum antenna is $v_i \mathbf{j}$. See fig. 12 for an illustration.

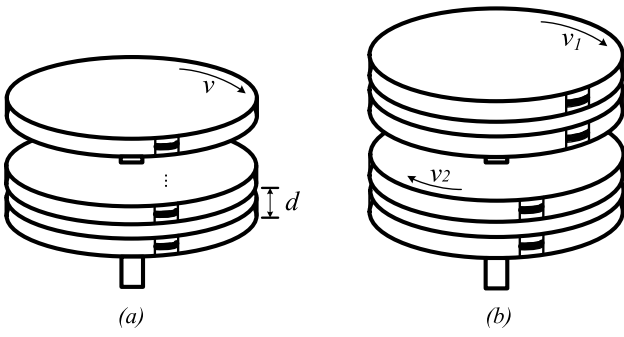


Fig. 11. (a) multi-antenna system for single-user communication and (b) multi-antenna system for multi-user configuration, where a setting for two-user system is shown to reduce the clutter.

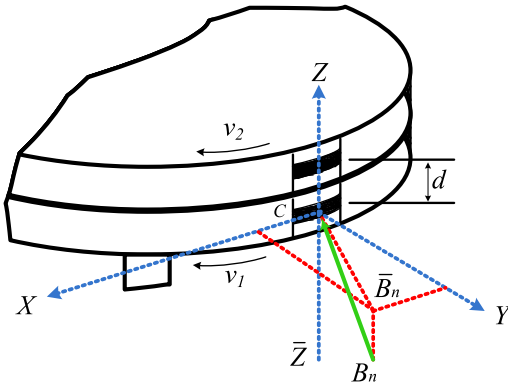


Fig. 12. An enlarged multi-antenna part-canister system that shows the azimuth and elevation of incoming rays. Only a single desired incoming ray, $B_n C \bar{Z} = \phi_n^S$ and $\bar{B}_n C Y = \beta_n^S$, is shown to reduce the clutter, where $B_n C \bar{Z} = \phi_n^S$ and $\bar{B}_n C Y = \beta_n^S$.

546 where $f_n^S = v_i \frac{f_c}{c} \sin \phi_n^S \sin \beta_n^S$, and $\psi_n^S \sim \mathcal{U}(0, 2\pi)$. Note
 547 that β_n^S and ϕ_n^S respectively are azimuth and elevation of the
 548 n th incoming ray measured in anti-clockwise direction with
 549 respect to CY and $C\bar{Z}$ axis respectively (see Fig. 12). Also,
 550 $\beta_n^S \sim \mathcal{U}(-\omega/2, \omega/2)$, and $\phi_n^S \sim \mathcal{U}(\pi/2 - \omega/2, \pi/2 + \omega/2)$,
 551 where it is assumed that both azimuth and elevation spread
 552 are the same. Note that 0th path denotes the dominant multi-
 553 path, and hence, $\beta_0^S = 0$, and it is also assumed that $\phi_0^S =$
 554 1.39626 which is 80° degrees and $d = 6\lambda_c = 3\text{cm}$. Similar
 555 fashion, $h_{Ii}(t)$ can also be obtained with the notable exception
 556 of $f_n^I = v_i \frac{f_c}{c} \sin \phi_n^I \sin(\theta + \beta_n^I)$. The ideal maximum ratio
 557 combining (MRC) can be achieved by:

$$\hat{r}(t) = (\mathbf{h}'_S(t))^H \mathbf{r}(t), \quad (29)$$

559 where $\hat{r}(t)$ is the combiner output and $(\mathbf{h}'_S(t))^H$ is the
 560 Hermitian conjugate of $\mathbf{h}'_S(t)$, $\mathbf{h}'_S(t) = \{h'_{S1}(t) h'_{S2}(t)\}^T$
 561 and also $\mathbf{r}(t) = \{r_1(t) r_2(t)\}^T$. However, often $h'_{Si}(t)$
 562 cannot be estimated exactly, and one reasonable remedy is to
 563 use \hat{h}_{Si} which is also used for data detection in (16), and note
 564 that the multi-antenna DAIM simulations in this section also
 565 employ \hat{h}_{Si} . Fig. 13 shows SIR_A performance after DAIM
 566 processing and combining, where T is the number of drum
 567 antennas configured as shown in Fig. 11-(a). It is clear that
 568 SIR_A improves significantly as T increases, and interestingly,
 569 one can manipulate the number of antennas, T , and the rotation
 570 speed, v , in order to achieve a certain SIR_A performance.

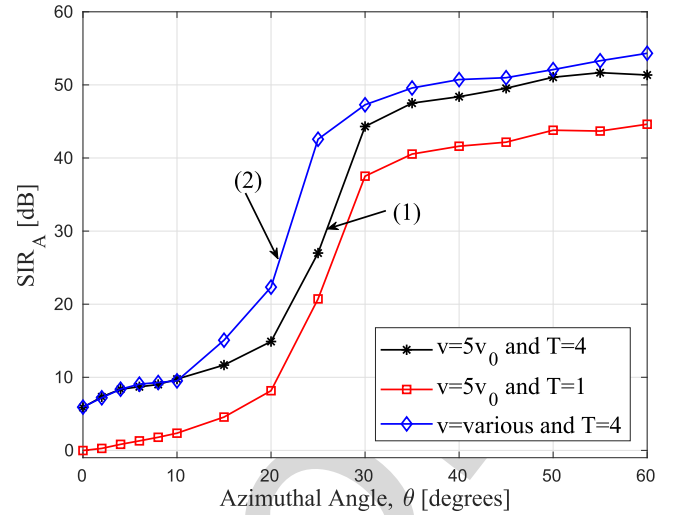


Fig. 13. SIR_A performance of multi-antenna DAIM for $SIR = 0$ dB, where $K = 10$ dB, $N = 20$, and $\omega = 10^\circ$. Note that $v_0 = \lambda_c B_w$.

It is anticipated that better channel estimation techniques shall
 571 increase SIR_A further. Note that all the drum antennas rotate
 572 at the same speed ($v = 5v_0$) for curve (1) in Fig. 13 which is
 573 not a necessary requirement.
 574

The Fig. 13 also shows (see curve (2)) the SIR_A perform-
 575 ance of a multi-antenna DAIM system with drums being
 576 rotated at different speeds of $v = 3v_0, 4v_0, 5v_0$, and $6v_0$. Let
 577 this speed profile be denoted as $\mathcal{SP}_2 = \{3v_0, 4v_0, 5v_0, 6v_0\}$.
 578 It is clear that SIR_A performance is always better than or the
 579 same as the case with drums being rotated at the same speed
 580 (i.e. a speed profile of $\mathcal{SP}_1 = \{v = 5v_0, 5v_0, 5v_0, 5v_0\}$). The
 581 energy required to rotate a single drum is proportional to the
 582 square of its angular velocity⁷ and in turn to the square of v .
 583 Hence, total energy, E_T required to rotate drum antennas in
 584 different profiles are:
 585

$$E_T \propto \begin{cases} 100v_0^2 & \mathcal{SP}_1, \\ 86v_0^2 & \mathcal{SP}_2, \end{cases} \quad (30)$$

and from kinetic energy efficiency perspective, \mathcal{SP}_2 is prefer-
 587 able as it is 14% more energy efficient than \mathcal{SP}_1 .
 588

B. Future Research

589 Even though the canister opening is directed to the direction
 590 of dominant scatters of the desired user, some non-dominant
 591 scatters can still induce fluctuations in the desired channel.
 592 Though these fluctuations can be harnessed to obtain some
 593 diversity gain as discussed in Sec. III-F, some deployments
 594 might prefer minimal channel fluctuations. Very closely and
 595 vertically placed oppositely rotating drum antennas could be
 596 used to reduce Doppler induced channel fluctuations. Note
 597 that this approach may not reduce Doppler shift in all fading
 598 conditions, and more research is required to understand the
 599 full potential of this approach. Furthermore, as shown in
 600 Fig. 11-(b), multi-antenna configuration can also be used for
 601 multi-user communication.
 602

⁷This is due to the fact that kinetic energy required to rotate a rigid body
 at certain angular velocity is $0.5I\omega^2$, where I is the moment of inertia and
 the angular velocity respectively.

The current paper discusses the basic operation of DAWC, and demonstrates the feasibility of it for CCI mitigation. We have herein used standard modulation techniques, channel estimation techniques, pulse shaping and filtering methods just to demonstrate the feasibility of the proposed system. It is expected that more tailored data modulation techniques [20], pulse shaping/filtering and also channel estimation techniques [21], [22] will increase the robustness and the performance of the proposed scheme.

It is also important to study other use cases of DAIM. In this paper, we have assumed that the interference occurs from a single interferer. If interference occurs from unknown number of interferers from unknown locations spread over a large azimuth, the state-of-the-art techniques like MIMO can be very ineffective due to their high reliance on CSI. However, DAIM, in these type of extremely hostile environments could be very effective.

V. CONCLUSIONS

The current paper has introduced, and studied a new class of systems termed as Doppler assisted wireless communication (DAWC in short). The proposed class of systems employs rotating drum antennas, and exploits Doppler effect, kinetic energy, and the topological information of wireless networks for CCI mitigation. This paper includes a detailed simulation study that models several important system and environmental parameters. The results presented herein show that difficult CCI—in the sense that it is statistically no more or less strong to the desired signal, and often poorly handled by existing interference mitigation techniques—can successfully be mitigated by the proposed system. This paper has also discussed several important phenomena occurred in DAWC systems such as Doppler gain along with advantages and challenges of DAWC.

REFERENCES

- [1] A. Osseiran *et al.*, "Scenarios for 5G mobile and wireless communications: The vision of the METIS project," *IEEE Commun. Mag.*, vol. 52, no. 5, pp. 26–35, May 2014.
- [2] J. Zander, "Distributed cochannel interference control in cellular radio systems," *IEEE Trans. Veh. Technol.*, vol. 41, no. 3, pp. 305–311, Aug. 1992.
- [3] M. Park and P. Gopalakrishnan, "Analysis on spatial reuse, interference, and MAC layer interference mitigation schemes in 60 GHz wireless networks," in *Proc. IEEE Int. Conf. Ultra-Wideband*, Vancouver, BC, Canada, Sep. 2009, pp. 1–5.
- [4] Z. Chen, C. Wang, X. Hong, J. Thompson, S. A. Vorobyov, and D. Yuan, "Cross-layer interference mitigation for cognitive radio MIMO systems," in *Proc. IEEE ICC*, Kyoto, Japan, Jun. 2011, pp. 1–6.
- [5] Z. Ding *et al.*, "Application of non-orthogonal multiple access in LTE and 5G networks," *IEEE Commun. Mag.*, vol. 55, no. 2, pp. 185–191, Feb. 2017.
- [6] Y. Saito *et al.*, "Non-orthogonal multiple access (NOMA) for cellular future radio access," in *Proc. IEEE VTC-Spring*, Dresden, Germany, Jun. 2013, pp. 1–5.
- [7] P. Marsch, M. Grieger, and G. Fettweis, "Large scale field trial results on different uplink coordinated multi-point (CoMP) concepts in an urban environment," in *Proc. IEEE WCNC*, Cancun, Mexico, Mar. 2011, pp. 1858–1863.
- [8] O. El Ayach, A. Lozano, and R. W. Heath, Jr., "On the overhead of interference alignment: Training, feedback, and cooperation," *IEEE Trans. Wireless Commun.*, vol. 11, no. 11, pp. 4192–4203, Nov. 2012.
- [9] L. C. Godara, "Application of antenna arrays to mobile communications. II. Beam-forming and direction-of-arrival considerations," *Proc. IEEE*, vol. 85, no. 8, pp. 1195–1245, Aug. 1997.

- [10] S. Haykin, "Cognitive radio: Brain-empowered wireless communications," *IEEE J. Sel. Areas Commun.*, vol. 23, no. 2, pp. 201–220, Feb. 2005.
- [11] D. A. Basnayaka *et al.*, "Doppler effect assisted interference mitigation for wireless communication," in *Proc. IEEE Global Commun. Conf.*, Abu Dhabi, UAE, 2018.
- [12] L. Lu *et al.*, "An overview of massive MIMO: Benefits and challenges," *IEEE J. Sel. Topics Signal Process.*, vol. 8, no. 5, pp. 742–758, Oct. 2014.
- [13] A. Paulraj *et al.*, "Introduction to Space-Time Wireless Communications," Cambridge, U.K.: Cambridge Univ. Press, 2003.
- [14] T. L. Koch and U. Koren, "Semiconductor lasers for coherent optical fiber communications," *J. Lightw. Technol.*, vol. 8, no. 3, pp. 274–293, Mar. 1990.
- [15] M. Gregory *et al.*, "TESAT laser communication terminal performance results on 5.6 Gbit coherent inter satellite and satellite to ground links," in *Proc. Int. Conf. Space Opt.*, Rhodes, Greece, Oct. 2010.
- [16] A. Goldsmith, *Wireless Communications*, Cambridge, U.K.: Cambridge Univ. Press, 2005.
- [17] G. L. Stüber, *Principles of Mobile Communication*, 2nd ed. Norwell, MA, USA: Kluwer, 2002.
- [18] D. A. Basnayaka, P. J. Smith, and P. A. Martin, "Performance analysis of macrodiversity MIMO systems with MMSE and ZF receivers in flat rayleigh fading," *IEEE Trans. Wireless Commun.*, vol. 12, no. 5, pp. 2240–2251, May 2013.
- [19] S. S. Haykin, *Adaptive Filter Theory*, 5th ed. London, U.K.: Pearson, 2013.
- [20] T. Dean, M. Chowdhury, and A. Goldsmith, "A new modulation technique for Doppler compensation in frequency-dispersive channels," in *Proc. IEEE PIMRC*, Montreal, QC, Canada, Oct. 2017, pp. 1–7.
- [21] P. Stoica and Y. Wang, *Spectral Analysis of Signals*, 1st ed. Upper Saddle River, NJ, USA: Prentice-Hall, 2005.
- [22] L. Zhao, G. Geraci, T. Yang, D. W. K. Ng, and J. Yuan, "A tone-based AoA estimation and multiuser precoding for millimeter wave massive MIMO," *IEEE Trans. Commun.*, vol. 65, no. 12, pp. 5209–5225, Dec. 2017.



Dushyantha A. Basnayaka (S'11–M'12–SM'18) received the B.Sc. Eng. degree (Hons.) and the Ph.D. degree in electrical and electronics engineering in 2006 and 2012, respectively. He is currently with the Institute for Digital Communications, The University of Edinburgh, U.K. His research interests include MIMO, physical layer aspects of IoT, and 5G. He holds two patents (one granted and one pending) in coordinated multi-point (CoMP) and IoT. He is a member of IEEE Communication Theory Society. He was a recipient of the University of Canterbury International Doctoral Scholarship from 2009 to 2012 and the Best Paper Award at the IEEE Vehicular Technology Conference (VTC-Spring) in 2015.



Tharmalingam Ratnarajah (A'96–M'05–SM'05) was the Head of the Institute for Digital Communications (2016–2018). He is currently with the Institute for Digital Communications, The University of Edinburgh, Edinburgh, U.K., as a Professor in digital communications and signal processing. His research interests include signal processing and information theoretic aspects of 5G and beyond wireless networks, full-duplex radio, mmWave communications, random matrices theory, interference alignment, statistical and array signal processing, and quantum information theory. He has published over 350 publications in these areas and holds four U.S. patents. He has raised over 15M € EU funding for numerous projects in many areas of wireless communication. He is a member of the American Mathematical Society and Information Theory Society and a fellow of the Higher Education Academy (FHEA). He was the Technical Co-Chair of the 17th IEEE International Workshop on Signal Processing Advances in Wireless Communications, Edinburgh, U.K., in 2016. He was an Associate Editor of the IEEE TRANSACTIONS ON SIGNAL PROCESSING (2015–2017).

Doppler Effect Assisted Wireless Communication for Interference Mitigation

Dushyantha A. Basnayaka¹, *Senior Member, IEEE*, and Tharmalingam Ratnarajah, *Senior Member, IEEE*

Abstract—Doppler effect is a fundamental phenomenon that appears in wave propagation, where a moving observer experiences dilation or contraction of the wavelength of a wave. It also appears in radio frequency (RF) wireless communication when there exists a relative movement between the transmitter and the receiver, and is widely considered as a major impairment for reliable wireless communication. The current paper proposes Doppler assisted wireless communication (DAWC) that exploits Doppler effect and uses kinetic energy for co-channel interference (CCI) mitigation. The proposed system also exploits the propagation environment and the network topology and consists of an access point (AP) with a rotating drum antenna. The rotating drum receive antenna is designed in such a way that it shifts the interfering signals away from the desired signal band. This paper includes a detailed system model, and the results show that under favorable fading conditions, CCI can be significantly reduced. Therefore, it is anticipated that more sophisticated wireless systems and networks can be designed by extending the basic ideas proposed herein.

Index Terms—Doppler effect, electromagnetic waves, co-channel interference, interference mitigation, kinetic energy.

I. INTRODUCTION

A MULTITUDE of wireless networks have revolutionized the modern living for a half a century, and are expected to revolutionize our lives in an unprecedented scale in the future too [1]. Today's wireless networks—often digital wireless networks—are used for various activities such as mass communication, security and surveillance systems, sensing and disaster monitoring networks, satellite communication and tactical communication systems. Wireless networks typically consist of a collection of wireless transmitters and receivers, and use a fixed band of radio frequency (RF) spectrum for communication. Due to spectrum scarcity, often wireless networks reuse their limited frequency spectrum, which in turn gives rise to a fundamental problem in wireless communication known as co-channel interference (CCI) [2].

The CCI occurs when wireless stations that are nearby use/reuse overlapping spectrum. Modern wireless networks widely employ many intelligent and adaptive physical (PHY)

layer interference mitigation/avoidance/management techniques such as interference detection and subtraction (also known as successive interference cancellation or SIC), coordinated multi-point systems (CoMP), interference alignment (IA), diversity receivers (such as maximal ratio combining (MRC), zero forcing (ZF) and minimum mean-squared error (MMSE)), cognitive radio (CR), cooperative communication and transmit power control. Often PHY layer techniques are more effective, but multiple access control (MAC) layer techniques such as schedule randomization, measurement and rescheduling, and super controller also exist [3]. Furthermore, cross layer techniques that combine and jointly optimize two or more MAC and PHY techniques for interference mitigation are also widely considered [4].

The PHY techniques add (or are expected to add) significant intelligence to future wireless networks. For instance, non-orthogonal multiple access systems (NOMA), which uses interference detection and subtraction along with power control is expected to increase the spectral efficiency and the system throughput in 5th generation (5G) mass communication networks [5], [6]. In CoMP, a number of co-channel transmitters provide coordinated transmission to multiple receivers and multiple receivers provide coordinated reception to multiple co-channel transmitters [7]. In IA, all the co-channel transmitters cooperatively align—by exploiting channel state information (CSI) at transmitters—their transmissions in such a way that the interference subspaces at all the receivers jointly are limited to a smaller dimensional subspace, and is orthogonal to the desired signal subspace [8]. Diversity receivers use multi-antenna techniques for interference mitigation [9], and CR learns from the environment, and adapts its transmission. If a particular channel is occupied by a primary user, CR halts transmission or transmits at a lower power level so that the possible interference to primary user is minimized [10].

The focus of this paper is also interference mitigation at PHY layer, where we envision to add a new degree of freedom to existing wireless receivers by exploiting Doppler effect. We introduce a new paradigm for wireless communication, namely Doppler Assisted Wireless Communication (DAWC in short) [11], and consider a receiver or an access point (AP) in a typical wireless sensor network with a circular high speed rotating drum antenna as shown in Fig. 1.

A. Rotating Drum Antenna

Fig. 1 illustrates the proposed circular drum antenna for DAWC. In order to exploit Doppler effect, the AP has a

Manuscript received July 16, 2018; revised December 19, 2018 and March 2, 2019; accepted April 6, 2019. This work was supported by the U.K. Engineering and Physical Sciences Research Council (EPSRC) under Grant EP/N014073/1. The associate editor coordinating the review of this paper and approving it for publication was A. Tajer. (*Corresponding author: Dushyantha A. Basnayaka.*)

The authors are with the Institute for Digital Communication, The University of Edinburgh, Edinburgh EH8 9YL, U.K. (e-mail: d.basnayaka@ed.ac.uk).

Color versions of one or more of the figures in this paper are available online at <http://ieeexplore.ieee.org>.

Digital Object Identifier 10.1109/TCOMM.2019.2912193

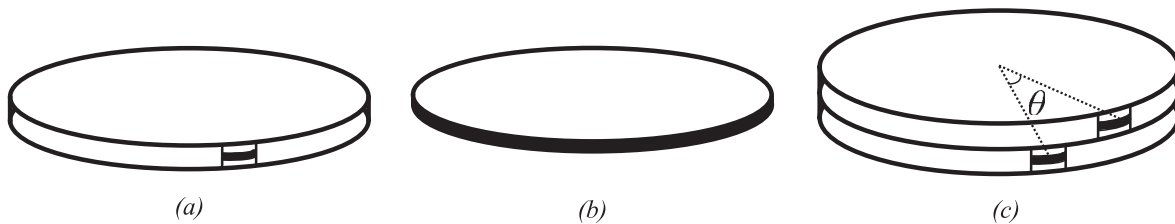


Fig. 1. A possible antenna implementation for Doppler assisted wireless communication (DAWC), where (a) a fixed antenna canister with an opening, where a small portion of the antenna is visible to outside, (b) a rotatable drum antenna, which is located inside the circular canister, (c) a possible implementation to receive two desired signals from two transmitters of azimuthal separation of θ .

86 circular antenna, which consists of two parts. 1) a fixed circular
 87 canister 2) a rotatable drum antenna as shown in Fig. 1-(b).
 88 The radiating surface of this conformal antenna lies on the
 89 curve surface of the drum, which is located inside the circular
 90 canister. There is an opening on the curve surface of the canis-
 91 ter, and it is directed to the direction of the desired transmitter.
 92 Consequently, the channel responses of the desired link and
 93 the other interfering links which have reasonable azimuthal
 94 separation exhibit different frequency characteristics. Despite
 95 Doppler effect being considered as a major impairment, the
 96 results in this paper indicate that successful receiver side CCI
 97 mitigation techniques (henceforth DAIM to denote Doppler
 98 assisted interference mitigation) can still be developed based
 99 on a rotating drum antenna and Doppler effect.

100 The round and/or rotating antenna units are used in several
 101 key widely-used systems such as TACAN (for tactical air
 102 navigation) and LIDAR (for light detection and ranging).
 103 The TACAN system has multiple antennas installed in a
 104 circle, and electronically steers a radio beam in order to
 105 provide directional information for distance targets over a
 106 360° azimuth. The radio beam rotates (often electronically)
 107 merely to serve targets located around it. However, the rotating
 108 antenna in DAWC is a key unit that gives rise to Doppler
 109 effect, and fundamentally important for the operation of
 110 the system. It typically rotates at very high speed than the
 111 beam in TACAN system. Furthermore, modern autonomous
 112 cars also employ a system known as LIDAR, which also
 113 has a rotating unit. LIDAR is a variation of conventional
 114 RADAR, and uses laser light instead of radiowaves to make
 115 high-resolution topological maps around automobiles. LIDAR
 116 antenna rotates in order merely to map 360° angle, and not
 117 for any other fundamental reason. The TACAN and LIDAR
 118 systems are hence fundamentally different from the system
 119 proposed in the current paper, and tackle entirely different
 120 challenges.

121 MIMO (or its more popular variant, massive MIMO) is
 122 the state-of-the-art for CCI mitigation, but heavily relies on
 123 CSI [12]. The proposed system does not rely on CSI for CCI
 124 mitigation (note however that, it still uses CSI of the desired
 125 user for data detection). Typically, CCI may occur from a
 126 single co-channel transmitter or numerous co-channel trans-
 127 mitters. If CCI occurs from multiple co-channel users, MIMO
 128 systems need fairly accurate CSI of all co-channel users for
 129 successful CCI mitigation [13]. They let the interference into
 130 the system, and uses ever more complex signal processing
 131 techniques (a software domain approach) for CCI mitigation.

In essence, massive MIMO lets the enemy (metaphorically
 to denote CCI) into its own backyard, and fight head-on.
 In contrast, the proposed system can handle any number of
 interferers, and automatically suppresses co-channel multi-
 path signals with a reasonable azimuthal separation to the
 desired multi-paths even before they corrupt the desired signal.
 In that sense, DAWC is a paradigm shifting technology, which
 keeps the enemy at the bay. Furthermore, the rotation is not a
 necessity. If CCI is not severe, and can be handled by software
 means, the antenna is not required to be rotated. The level of
 CCI mitigation can be controlled rapidly by simply changing
 the rotation speed of the antenna. In essence, DAWC adds a
 new degree of freedom to future wireless APs.

It is important to note furthermore that, the results in
 this paper are also applicable to wireless networks based on
 microwave, mmwave frequencies, and also to coherent optical
 laser communication systems [14], [15].

This paper includes a detailed study of DAWC on
 MATLAB. The rest of the paper also includes the system
 model in Sec. II, performance analysis and discussions in
 Sec. III, further remarks in Sec. IV, and conclusions in Sec. V.

II. SYSTEM MODEL

A narrow-band uplink communication from a wireless sta-
 tion, S (to denote source) to AP in a wireless network is
 considered, where another wireless station, I (to denote the
 interferer) located at an azimuthal angle separation of θ poses
 CCI as shown in Fig. 2. Note that, all wireless stations are
 fixed, and both S and I are in transmit mode while AP being
 in receive mode. It is assumed that AP has a rotating drum
 antenna of radius, R , with the canister opening being directed
 towards the desired transmitter, S . Let the analog complex
 baseband signal of the desired and the interfering stations
 respectively be given by $b_S(t)$ and $b_I(t)$:

$$b_S(t) = \Psi(a_S), \quad (1)$$

$$b_I(t) = \Psi(a_I), \quad (2)$$

where a_S and a_I respectively are the complex discrete time
 base-band data—drawn from a M -Quadrature Amplitude Mod-
 ulation (M -QAM) constellation, \mathcal{M} based on binary data
 signals, d_S and d_I —signals of stations, S and I and the
 operation $\Psi(\cdot)$ denotes the square root raised cosine (SRRC)
 pulse shaping operation [16]. Let the symbol time duration
 and the bandwidth of the data signals be denoted by T_s and
 B_w respectively, where typically $T_s = 1/B_w$. The transmit

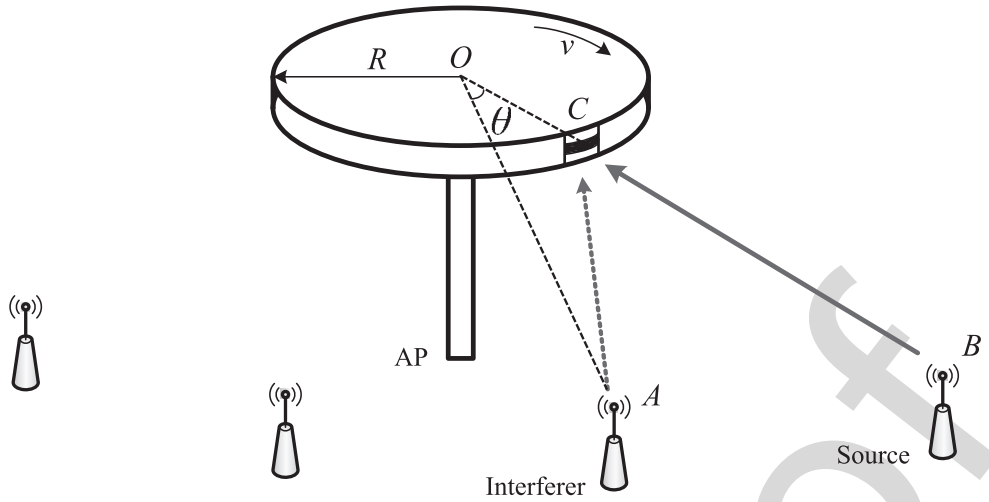


Fig. 2. A wireless AP with a single rotating antenna for DAWC. The figure is not to the scale, and the AP is exaggerated for exposition. To reduce the clutter, not all wireless links are shown.

175 waveforms will then be given by:

$$176 \quad x_S(t) = \text{Re} \{ b_S(t) e^{j2\pi f_c t} \}, \quad (3)$$

$$177 \quad x_I(t) = \text{Re} \{ b_I(t) e^{j2\pi f_c t} \}, \quad (4)$$

178 where f_c is the carrier frequency, $j = \sqrt{-1}$, and $\text{Re} \{ \}$ denotes
 179 the real part [17]. Furthermore, the transmit power of both
 180 links are scaled to give $\mathcal{E} \{ x_S(t)^2 \} = P_S$ and $\mathcal{E} \{ x_I(t)^2 \} =$
 181 P_I . It is herein assumed that the communication takes place
 182 between S , I and AP in a scattering environment, where AP
 183 receives multiple faded replicas of the transmitted signals,
 184 $x_S(t)$ and $x_I(t)$. Hence, the received signal by AP can in
 185 the absence of noise be given by:

$$186 \quad y(t) = \text{Re} \{ r_S(t) e^{j2\pi f_c t} \} + \text{Re} \{ r_I(t) e^{j2\pi f_c t} \}, \quad (5)$$

187 where the complex base-band desired and interfering received
 188 signals, $r_S(t)$ and $r_I(t)$ can be given by:

$$189 \quad r_S(t) = \sum_{n=0}^{N_S} \alpha_n^S e^{j\phi_n^S(t)} b_S(t - \tau_n^S), \quad (6a)$$

$$190 \quad r_I(t) = \sum_{n=0}^{N_I} \alpha_n^I e^{j\phi_n^I(t)} b_I(t - \tau_n^I). \quad (6b)$$

191 The quantities, α_n , ϕ_n and τ_n in (6) respectively are the faded
 192 amplitude, phase and path delay of the n th replica of the
 193 desired and interference signals, where:

$$194 \quad \phi_n^S(t) = 2\pi \{ f_n^S t - (f_c + f_n^S) \tau_n^S \}, \quad (7a)$$

$$195 \quad \phi_n^I(t) = 2\pi \{ f_n^I t - (f_c + f_n^I) \tau_n^I \}. \quad (7b)$$

196 It is assumed that α_n^S , α_n^I , τ_n^S , τ_n^I , N_S and N_I are approx-
 197 imately the same for a certain amount of time (say block
 198 interval) that is sufficient to transmit at least one data packet,
 199 and change to new realizations independently in the next block
 200 interval. The frequency change due to Doppler effect on the
 201 n th incoming ray of the desired and the interfering signal, f_n^S
 202 and f_n^I in (7) are respectively given by:

$$203 \quad f_n^S = f_m \sin(\beta_n^S), \quad (8a)$$

$$204 \quad f_n^I = f_m \sin(\theta + \beta_n^I), \quad (8b)$$

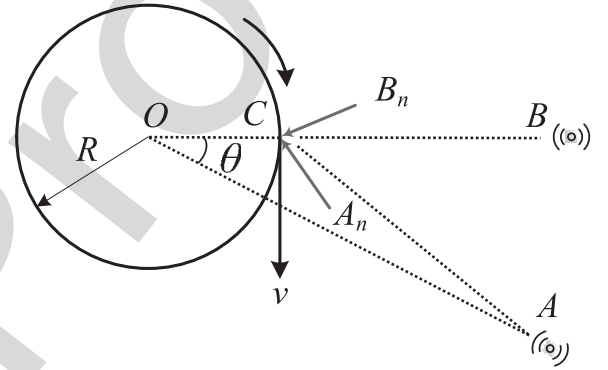


Fig. 3. The top view of an access point, where one desired (i.e. B_nC) and one interfering ray (i.e. A_nC) are shown. The canister opening is at C .

205 where $f_m = f_c v / C$. Note that the arrival angles of users
 206 are measured with respect to the direction of the respective
 207 user. For instance, the arrival angles, β_n^S of the desired
 208 user are measured with respect to the direction of CB (see
 209 Fig. 3), and the arrival angles, β_n^I of the interfering user
 210 are measured with respect to the direction of CA . As a result,
 211 according to Fig. 3, the n th angle of arrival of the desired
 212 and the interfering signals are given by $\beta_n^S = \angle BCB_n$ and
 213 $\beta_n^I = \angle ACA_n$. Furthermore, the dominant angles of arrivals
 214 are limited to $-\omega/2 \leq \beta_n^S, \beta_n^I \leq \omega/2$ for all n . Since
 215 it is a narrow-band communication link, we further assume
 216 that $\tau_n^S, \tau_n^I \ll T_s$, and with out loss of applicability, make
 217 the substitution, $\tau_S \approx \tau_n^S$ and $\tau_I \approx \tau_n^I$ for all n . As a
 218 result:

$$219 \quad r_S(t) = b_S(t - \tau_S) \sum_{n=0}^{N_S} \alpha_n^S e^{j\phi_n^S(t)}, \quad (9a)$$

$$220 \quad r_I(t) = b_I(t - \tau_I) \sum_{n=0}^{N_I} \alpha_n^I e^{j\phi_n^I(t)}, \quad (9b)$$

One must note that the approximations, $\tau_S \approx \tau_n^S$ and $\tau_I \approx \tau_n^I$ are invoked only to $b_S(t - \tau_n^S)$ and $b_I(t - \tau_n^I)$ in (9), and since, $f_c \tau_n^S$ and $f_c \tau_n^I$ can still be significant, the path delay differences are still considered in the summation of (9). If the perfect synchronization is assumed, the complex baseband desired and interfering received signals, $r_S(t)$ and $r_I(t)$ can be rewritten as:

$$r_S(t) = \left\{ \sum_{n=0}^{N_S} \alpha_n^S e^{j\phi_n^S(t)} \right\} b_S(t) = h_S(t) b_S(t), \quad (10a)$$

$$r_I(t) = \left\{ \sum_{n=0}^{N_I} \alpha_n^I e^{j\phi_n^I(t)} \right\} b_I(t) = h_I(t) b_I(t), \quad (10b)$$

where $h_S(t)$ and $h_I(t)$ are denoted henceforth as channel fading functions. The averaged channel gains for both links are defined as $\mathcal{E} \{|h_S(t)|^2\} = g_S$ and $\mathcal{E} \{|h_I(t)|^2\} = g_I$ [18]. The constants, g_S and g_I capture the average channel gains due to path loss and shadowing alone which is also given by $g_S = \mathcal{E} \left\{ \sum_{n=0}^{N_S} (\alpha_n^S)^2 \right\}$ and $g_I = \mathcal{E} \left\{ \sum_{n=0}^{N_I} (\alpha_n^I)^2 \right\}$, where the expectation is over block intervals.

It is assumed that dominant (in terms of the receive power) paths exist from both source and interferer to AP either as a result of line-of-sight (LoS) or dominant non-line-of-sight (NLoS) rays along with significantly weaker scattered rays. With out loss of generality, let the 0th terms in (6) denote the dominant paths, and as also pointed out earlier, AP points the canister opening towards dominant paths from S . Let K be Rician K -factor which models the ratio of the received power between the dominant path and other paths [16]. Then:

$$K = \frac{\mathcal{E} \left\{ (\alpha_0^S)^2 \right\}}{\mathcal{E} \left\{ \sum_{n=1}^{N_S} (\alpha_n^S)^2 \right\}} = \frac{\mathcal{E} \left\{ (\alpha_0^I)^2 \right\}}{\mathcal{E} \left\{ \sum_{n=0}^{N_I} (\alpha_n^I)^2 \right\}}, \quad (11)$$

where it is assumed that K -factor is the same for both the desired and interference link. The received signal in the presence of noise is given by:

$$y(t) = \text{Re} \left\{ [r_S(t) + r_I(t) + n(t)] e^{j2\pi f_c t} \right\}, \quad (12)$$

where $n(t)$ is complex base-band zero mean additive white Gaussian noise (AWGN) signal with $\mathcal{E} \{|n(t)|^2\} = \sigma_n^2$. The signal-to-noise-ratio is hence defined as $\text{SNR} = g_S P_S / \sigma_n^2$, and signal-to-interference power ratio is defined as $\text{SIR} = g_S P_S / g_I P_I$. The AP processes the received signal, $y(t)$ by in-phase and quadrature-phase mixing and filtering with a low pass filter (LPF) of bandwidth, B_w to obtain the continuous-time complex base-band equivalent received signal as:

$$r(t) = r'_S(t) + r'_I(t) + n(t). \quad (13)$$

One must distinguish the difference between $r_S(t)$ and $r'_S(t)$ (also between $r_I(t)$ and $r'_I(t)$) in (13) that $r'_S(t)$ is the low pass filtered version of $r_S(t)$ which is the original faded desired signal supposed to be received by AP. Conventionally, LPF assures that $r'_S(t) = r_S(t)$ and $r'_I(t) = r_I(t)$. However as v increases, and also discussed in detail in Sec. II-A, $r_S(t)$ and $r_I(t)$ broaden in the frequency domain due to Doppler effect. Since the canister is directed towards the

desired source, the spectral broadening in $r_S(t)$ is less severe, and under favorable fading conditions, reliable communication is still possible with a reasonable channel estimation overhead. Moreover, if v is sufficiently large, the spectrum of $r_I(t)$ shifts to an intermediate frequency determined by v and θ . Consequently, a majority or entire interference signal, $r_I(t)$, can be made to be filtered out by LPF so to create a less interfered channel. The AP samples $r(t)$ at symbol rate to obtain the discrete time complex base-band signal in terms of desired data signal, a_S as:

$$r(\ell) = r'_S(\ell) + n'(\ell), \quad (14a)$$

$$= h'_S(\ell) a_S(\ell) + n'(\ell), \quad \forall \ell \quad (14b)$$

where ℓ alone is used for ℓT_s . Furthermore, $r'_S(\ell)$ and $n'(\ell)$ are the sampled versions of $r'_S(t)$ and $r'_I(t) + n(t)$ respectively. Note that $h'_S(\ell)$ combines the effect of $h_S(\ell)$ and other possible effects of low pass filtering of $r_S(\ell)$. The detector then uses the following symbol-by-symbol detection rule based on minimum Euclidean distance (also equivalent to maximum likelihood (ML) detector in AWGN) which treats the interference plus noise, $n'(\ell)$, as additional noise to obtain the estimated data, \hat{d}_S :

$$\hat{d}_S(\ell) = \min_{a_S(\ell) \in \mathcal{M}} |r(\ell) - h'_S(\ell) a_S(\ell)|^2, \quad \forall \ell. \quad (15)$$

Unlike in the case with $v = 0$, due to Doppler effect, $h'_S(\ell)$ are different within a block interval even with $\alpha_n, \phi_n, \tau_n, N_S$ and N_I being fixed. However, in this study, we assume that they can be approximated by a fixed value, \hat{h}_S . Consequently, (15) becomes:

$$\hat{d}_S(\ell) = \min_{a_S(\ell) \in \mathcal{M}} |r(\ell) - \hat{h}_S a_S(\ell)|^2, \quad \forall \ell. \quad (16)$$

where \hat{h}_S is the estimated value of h_S . The key roles played by spectral characteristics of channel fading functions in (10) are graphically discussed in the next section.

A. The Effects of Antenna Rotation

Conventionally, the antenna is fixed (i.e. $v = 0$), but as rotation speed increases, two conflicting phenomena happen. These phenomena can be better explained using the illustrations in Fig. 4. The Fig. 4-(a) shows an illustration of the single-sided magnitude response of $r_S(t)$, $r_I(t)$, $h_S(t)$ and $h_I(t)$ along with the magnitude response of the receiver's LPF. When $v = 0$, $H_S(f)$ and $H_I(f)$ are just impulses, and have no relevant effect on $r_S(f)$ and $r_I(f)$. However, as v increases $H_S(f)$ and $H_I(f)$ tend to broaden, and notably, $H_I(f)$ sways away from zero frequency (i.e., $f = 0$) to an intermediate frequency determined by $f_D = f_m \sin \theta$, and in turn by the azimuthal separation, θ , v , and f_c . Consequently, the majority of interference power lies outside the desired signal bandwidth, B_w , and hence, there is an interference suppression effect. On the other hand, since, $R_S(f) = H_S(f) \otimes B_S(f)$ and $R_I(f) = H_I(f) \otimes B_I(f)$, $R_S(f)$ and $R_I(f)$ also tend to broaden. Note that $B_S(f)$ and $B_I(f)$ denote the frequency response of $b_S(t)$ and $b_I(t)$ respectively, and \otimes denotes the convolution operator [16]. As a result of

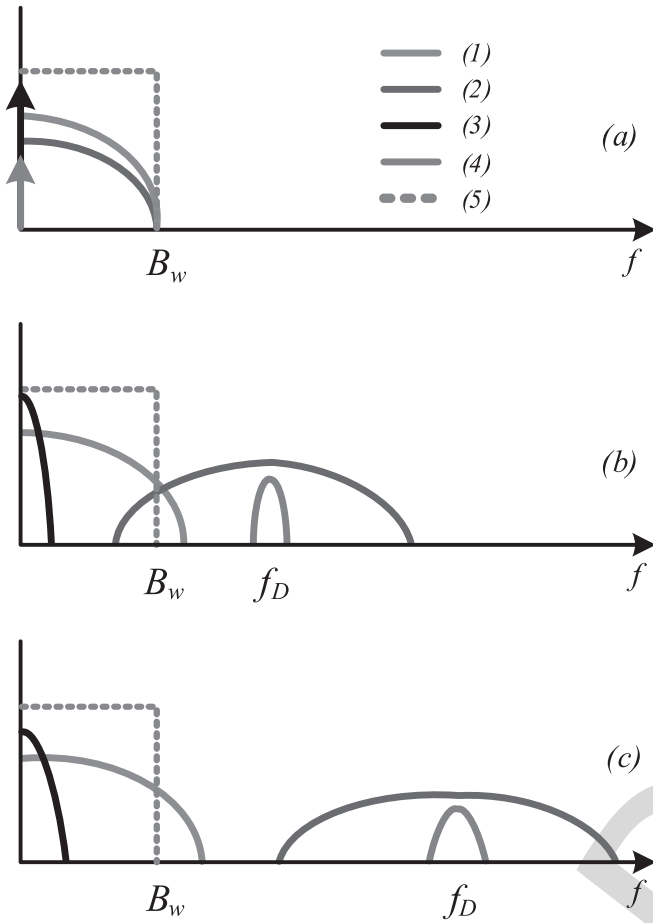


Fig. 4. Illustrations of magnitude responses of (1) $R_S(f)$, (2) $R_I(f)$, (3) $H_S(f)$ and (4) $H_I(f)$ which are Fourier transforms of $r_S(t)$, $r_I(t)$, $h_S(t)$ and $h_I(t)$ respectively. The magnitude response of LPF at AP is also shown in (5), and $f_D = \frac{v f_c}{C} \sin \theta$.

320 this spectrum broadening,¹ a certain amount of desired signal
 321 power is also suppressed by LPF and thus a distortion effect
 322 on the desired signal. As v increases further, as shown in
 323 Fig. 4-(c), the interference signal can be shifted completely
 324 away from the desired signal, but the amount of power
 325 suppressed by the LPF also increases making the desired
 326 signal more distorted. Hence, a trade off between interference
 327 suppression capability and the distortion of the desired signal
 328 in DAWC is clearly apparent. However, as shown in Sec. III-F,
 329 a reasonable compromise can be made, where a significant
 330 performance gain can still be achieved.

331 III. PERFORMANCE ANALYSIS AND DISCUSSION

332 The performance of DAIM (a convenient name for DAWC
 333 when applied for CCI mitigation) is analyzed using a compre-
 334 hensive end-to-end digital communication link simulated on
 335 MATLAB. In order to accurately assess DAIM, we herein
 336 simulate a pass-band digital communication link, where
 337 pulse shaping, up-conversion, RF mixing and LPF have also

¹The spectral broadening is initiated by the rotation, but could be exacerbated by adverse fading conditions such as low K , and high N_S , N_I and w .

TABLE I
NOTATIONS AND THEIR DEFINITIONS

Definition	Symbol
Carrier frequency	f_c
Speed of light	C
Sampling frequency	F_s
Signal bandwidth	B_w
Symbol duration	T_s
Rician factor	K
Number of S/I multi-path components	N_S/N_I
Amplitude of the n th S/I multi-path	α_n^S/α_n^I
Phase of the n th S/I multi-path	ϕ_n^S/ϕ_n^I
Delay of the n th S/I multi-path	τ_n^S/τ_n^I
Azimuthal separation of S and I	θ

338 been implemented.² The main block diagram of the simulation
 339 is shown in Fig. 5, where for simplicity Quadrature Phase Shift
 340 Keying (QPSK) is considered with other system parameters as
 341 shown in Tables I and II. The major steps of the simulation
 342 environment are obtained as follows.

343 A. Transmit Signals

344 We consider a time duration to transmit a single data packet,
 345 where a single packet lasts L symbols or equivalently ηL
 346 samples. The constant, η denotes the up-sampling ratio, which
 347 is given by $\eta = T_s/t_o$, where $t_o = 1/F_s$ is the sampling
 348 period in the computer simulation herein. The k th sample of
 349 the complex base-band transmitted signal of the desired link³
 350 is obtained by:

$$b_S(kt_o) = [\tilde{a}_S \otimes p](kt_o), \quad k = 1, \dots, \eta L, \quad (17)$$

352 where \tilde{a}_S is the k th sample of up-sampled version of a_S and
 353 $p(kt_o)$ is the k th sample of SRRC filter which is obtained
 354 by:

$$p(kt_o) = \frac{\sin(\pi k(1-\rho)) + 4\pi k \cos(\pi k(1+\rho))}{\pi k(1-16k^2\rho^2)}, \quad (18)$$

356 where ρ is the roll-off factor of SRRC filter. Henceforth,
 357 we may interchangeably use standalone k for kt_o . Fur-
 358 thermore, we scale $b_S(kt_o)$ so $\mathcal{E}\{|x_S(k)|^2\} = P_s/\eta =$
 359 $1/\eta$. Consequently, the k th sample of the normalized com-
 360 plex base-band faded desired received signal⁴ is obtained
 361 by:

$$r_S(k) = b_S(k) h_S(k). \quad (19)$$

²Note that the implementation of up-conversion and RF mixing which requires a significantly higher sampling rate, and hence is computationally inefficient, is avoided by using an equivalent base-band model, but still with transmit pulse shaping and LPF in order to accurately captures the effects outlined in Sec. II-A. Unlike in conventional complex base-band simulations, the LPF operation is crucial for this simulation study.

³Note that one can obtain the k th sample of the pass-band transmit signal of the desired link by $x_S(kt_o) = b_S(kt_o) e^{j2\pi f_c kt_o}$.

⁴Note that one can obtain the k th sample of the complex pass-band desired received signal by $\text{Re}\{r_S(k) e^{j2\pi f_c k}\}$.

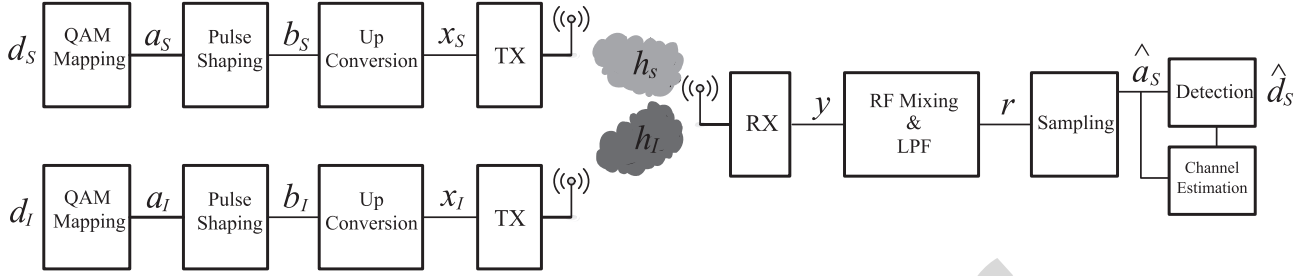


Fig. 5. The main simulation block diagram.

B. Multi-Path Channels

The k th sample of the fading function, $h_S(k)$ is obtained by the complex equation:

$$h_S(k) = \sqrt{\frac{g_S K}{K+1}} [h_S]_d + \sqrt{\frac{g_S}{K+1}} [h_S]_s, \quad (20)$$

where the channel function of the direct path of the desired link, $[h_S]_d = e^{-j\varphi_0^S}$, and the channel function of the scattered paths, $[h_S]_s$ is obtained as:

$$[h_S]_s = \sum_{n=1}^{N_S} \alpha_n^S e^{j2\pi f_n^S k t_o - j\psi_n^S}. \quad (21)$$

The term that accounts for the change in the frequency due to Doppler effect, f_n^S is obtained by $f_n^S = f_m \sin(\beta_n^S)$, where $\beta_n^S \sim \mathcal{U}(-\omega/2, \omega/2)$. Note that $\mathcal{U}(a, b)$ is an abbreviation for the uniform distribution with support, $[a, b]$. The phase term, ψ_n^S is obtained by $\psi_n^S \sim \mathcal{U}(0, 2\pi)$. More importantly, note that $f_0^S = 0$ for any v due to the fact that canister opening is directed towards to the desired transmitter. Furthermore, in LoS fading, ψ_0^S is dependent on the distance between S and AP, and hence is set to a fixed arbitrary value throughout the simulation. Lastly, the amplitudes, α_n^S are assumed to be approximately equal, and hence, are set to $\alpha_n^S = \sqrt{1/2N_S}$ which in conjunction with (20) subsequently guarantees that $\mathcal{E}\{|h_S(k)|^2\} = g_S$. This along with the fact that $\mathcal{E}\{|x_S(k)|^2\} = 1/\eta$ directly implies that $\mathcal{E}\{|r_S(k)|^2\} = 1/\eta$. Similarly, the k th sample of the scattered received signal of the interfering link, $r_I(k t_o)$ is also obtained with following notable exceptions: $[h_S]_d = e^{j2\pi f_0^I - j\psi_0^I}$, where $f_0^I = f_m \sin \theta$. Furthermore, β_n^I and ψ_n^I are assumed to be distributed as in the case for the desired link.

C. Receive Signal at AP

As a result, the k th sample of the combined pass-band received signal by AP is obtained as:

$$y(k) = \text{Re}\{[r_S(k) + r_I(k) + n(k)]e^{j2\pi f_c k}\}, \quad (22)$$

where $n(k)$ is the k th AWGN sample with variance σ_n^2/η , and since $r_S(k)$ and $r_I(k)$ are normalized to have average channel gains, g_S and g_I respectively, SIR of the wireless network boils down to $\text{SIR} = g_S/g_I$, and can be adjusted conveniently by manipulating, g_S and g_I in the computer simulation herein. Furthermore, SNR also boils down to $\text{SNR} = g_S/\sigma_n^2$.

D. RF Mixing, LP Filtering, Sampling and Detection

It is assumed herein that AP performs I/Q mixing perfectly,⁵ and produces a base-band version of $y(k)$, which is $r_S(k) + r_I(k) + n(k)$. The AP then passes this complex base-band version of $y(k)$ through SRRRC LPF. The low pass filtered complex signal is then sampled (rather down-sampled) at symbol rate of T_s to obtain $r(\ell T_s)$, for $\ell = 1, \dots, L$, which are the faded, interfered and noisier versions of the complex modulated samples, $a_S(\ell T_s)$, $\forall \ell$. The L complex samples per packet are then forwarded to the detector in (16) to obtain the reproduced data, \hat{d}_S .

E. Simple Channel Estimation

As pointed out in Sec. II, despite being different, all fading coefficients, $h'_S(\ell)$ s, in a single data packet duration are approximated by a single value, \hat{h}_S . In this study, we assume that the desired transmitter sends Q number of known data symbols, and AP uses simple least-square (LS) algorithm for channel estimation [19]. From (14), the complex base-band signal received in the channel estimation phase, $r^e(\ell)$, is:

$$r^e(\ell) = h'_S(\ell) a_S^e(\ell) + n'(\ell), \quad \text{for } \ell = 1, \dots, Q, \quad (23)$$

$$\approx \hat{h}_S a_S^e(\ell) + n'(\ell), \quad (24)$$

where $a_S^e(\ell)$ are known symbols transmitted for channel estimation. The LS estimation of \hat{h}_S can hence be obtained as: $\hat{h}_S = (\mathbf{a}_S^e)^H \mathbf{r}^e / (\mathbf{a}_S^e)^H \mathbf{a}_S^e$, where $\mathbf{r}^e = \{r^e(1), \dots, r^e(Q)\}^T$ and $\mathbf{a}^e = \{a_S^e(1), \dots, a_S^e(Q)\}^T$. In the forthcoming simulation study, $Q = 8$ is used.

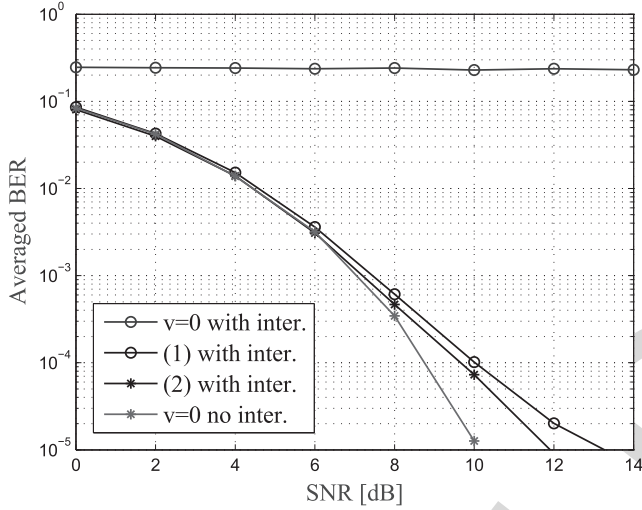
F. Simulation Results

A severely interfered link is simulated, where both desired and interference links have equal average link gains, so $g_I = g_S$. Hence, the SIR before the DAIM receiver denoted herein as SIR is 0 dB. Fig. 6 shows the averaged BER performance of a communication link with SIR = 0 dB, $N_S = N_I = 50$, $K = 20$ dB, and $\omega = 20^\circ$, where the results show that when $v = 0$, the link with interference is completely unusable. However, as v increases to $v = 2.5\lambda_c B_w$, BER performance improves significantly. BER performance with no interference and $v = 0$ is also shown for comparison. It is apparent that at low SNR, DAIM can create an interference free link, but

⁵Note that one can obtain the k th sample of the in-phase mixed signal by $y(k) \cos 2\pi f_c k$ while $y(k) \sin 2\pi f_c k$ being the quadrature phase mixed signal.

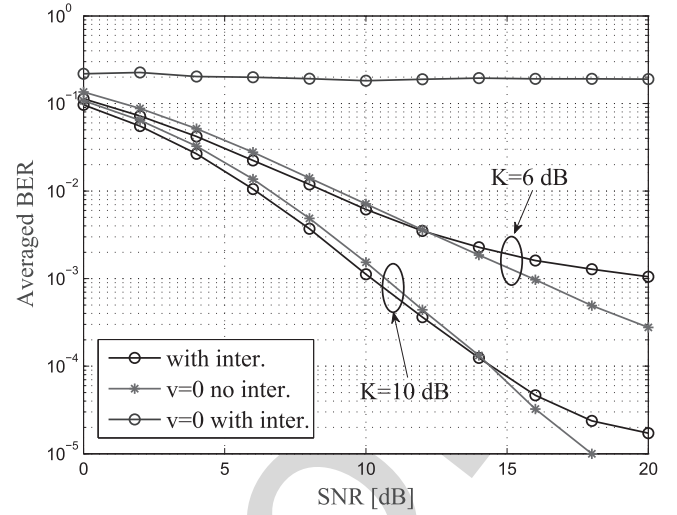
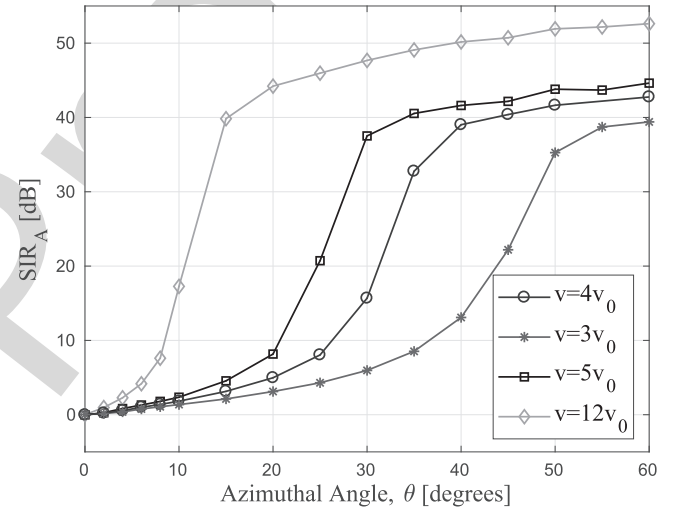
TABLE II
 PARAMETERS FOR QPSK PASS-BAND SIMULATION

Parameter	Value
Carrier frequency, f_c	60 GHz
Sampling frequency, F_s	3 MHz
Signal bandwidth, B_w	5 KHz
Symbol duration, T_s	$1/B_w$
Low pass filter	SRRC
SRRC span	$64T_s$
Rolloff factor of SRRC, ρ	0.2
Over sampling rate, η ,	300
Packet Length, L	$500T_s$


 Fig. 6. BER performance of DAIM, where $SIR = 0$ dB, $K = 20$ dB, $N = 50$, $\omega = 20^\circ$, and v is set such that in (1), $f_D = 10.8$ KHz and in (2), $f_D = 12.9$ KHz.

438 as SNR increases, BER performance drifts away. This trend
 439 can be attributed to the phenomenon that as v increases, the
 440 spectrum of the desired signal $h_S(t)b_S(t)$ broadens, which
 441 in turn makes a certain amount of desired signal power
 442 suppressed by LPF at AP.

443 Fig. 7 shows BER performance of the proposed interference
 444 mitigation system with $SIR = 0$ dB, $N = 20$, $K = 6/10$ dB
 445 and $\omega = 10^\circ$. As v increases, similar to Fig. 6, BER
 446 performance significantly improves specially at low SNR.
 447 As SNR increases BER performance again drifts away from
 448 BER performance of the completely interference free link.
 449 In this fading condition, two major factors come into effect.
 450 The first one is the effect that in low K values, the spectral
 451 broadening of $h_S(t)$ is severe, and hence a relatively larger
 452 amount of power is suppressed by LPF. The second one is
 453 the channel estimation errors. In the absence of significantly
 454 dominant multi-path components, the volatility of $h_S(t)$ even
 455 in the time duration of a single packet may be considerable.
 456 Approximating $h_S(\ell)$ for all ℓ s by a single \bar{h}_S is obviously
 457 suboptimal, and hence, more tailored algorithms for desired
 458 channel estimation may be needed. Furthermore, it is anti-
 459 cipated that more scenario specific low pass filters that passes
 460 a majority of desired signal power will be more effective for
 461 the earlier challenge as well.


 Fig. 7. BER performance of DAIM, where $SIR = 0$ dB, $K = 6/10$ dB, $N = 20$, $\omega = 10^\circ$ degrees, and v , when rotating, is set such that $f_D = 17.3$ KHz.

 Fig. 8. SIR_A performance of DAIM for $SIR = 0$ dB, where $K = 10$ dB, $N = 20$, and $\omega = 10^\circ$. Note that $v_0 = \lambda_c B_w$.

462 Fig. 7 also shows that BER of DAIM is marginally better
 463 than BER of interference free link with $v = 0$. This gain,
 464 though small, is defined as *Doppler Gain (DG)*. Doppler effect
 465 causes the fading function, $h_S(t)$, to fluctuate specially in low
 466 K and high N_S and ω . As a result, certain fading coefficients,
 467 $h_S(\ell)$, enhance their respective data symbols. Consequently,
 468 a net BER gain, which is manifested in the BER performance
 469 as DG, can be achieved. The simulation results that do not
 470 appear in this paper for reasons of space also show that
 471 ideal channel state information of the desired link significantly
 472 increases both BER of DAIM and DG.

473 Fig. 8 shows another view point of CCI mitigation capability
 474 of DAWC. Let the SIR after DAIM be denoted by SIR_A ,
 475 and:

$$476 \quad SIR_A = \frac{\mathcal{E}\{|r'_S(t)|^2\}}{\mathcal{E}\{|r'_I(t)|^2\}}, \quad (25)$$

477 where $r'_S(t)$ and $r'_I(t)$ are given in (13). Fig. 8 shows the
 478 SIR_A performance of DAIM against the azimuthal separation,
 479 θ for different rotation speeds. It can be seen here that higher

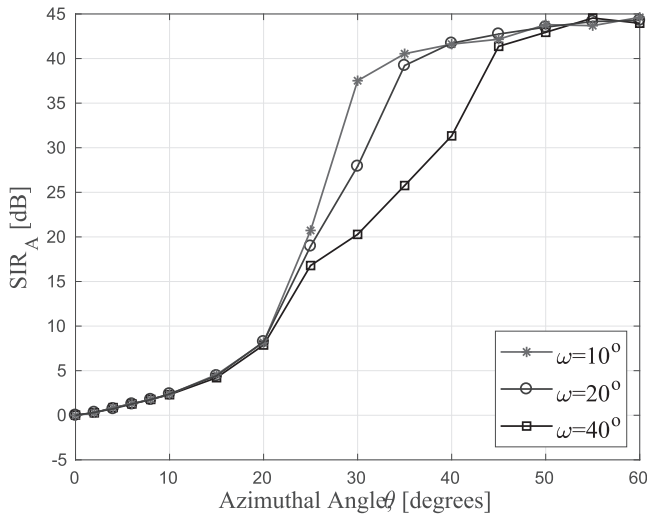


Fig. 9. SIR_A performance of DAIM for $SIR = 0$ dB, where $K = 10$ dB, $N = 20$, and $\omega = 10^\circ/20^\circ/40^\circ$. Note that $v = 5v_0$.

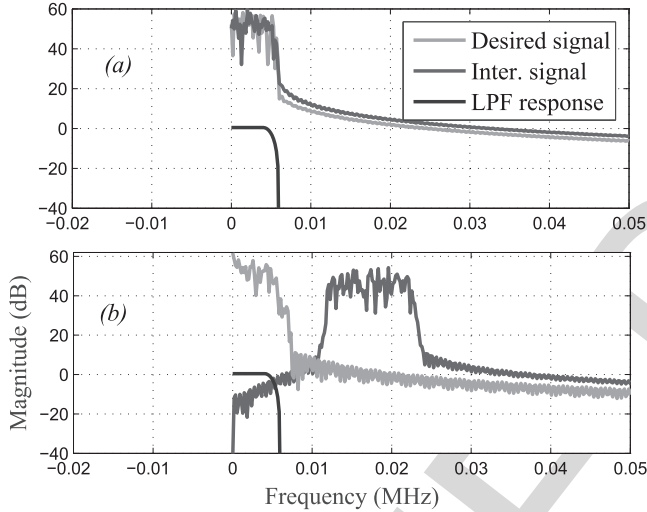


Fig. 10. Spectral characteristics of faded signals, $h_S(t)b_S(t)$ and $h_I(t)b_I(t)$, where $SIR = 0$ dB, $K = 10$ dB, $N = 20$, $\omega = 10^\circ$ degrees. In (a) $v = 0$ and in (b), v is set such that $f_D = 17.3$ KHz.

rotation speed may be required to achieve a certain SIR_A for low θ s and vice versa. Furthermore, Fig. 9 shows SIR_A performance of DAIM for various angle spreads ($\omega = 10^\circ/20^\circ/40^\circ$) for a fixed rotation speed of $v = 5v_0$, where $v_0 = \lambda_c B_w$.

Fig. 10-(a) and (b) show the spectral characteristics of faded signals, $h_S(t)b_S(t)$ and $h_I(t)b_I(t)$ with static and rotating antenna respectively. Herein, we consider a fading scenario, where $SIR = 0$ dB, $K = 10$ dB, $N = 20$, $\omega = 10^\circ$ degrees, and v is set, when rotating, such that $f_D = 17.3$ KHz. The figure clearly shows that as v increases, the interference signal, $h_I(t)b_I(t)$ shifts to an intermediate frequency so that it is suppressed by LPF. Furthermore, the spectral broadening, as v increases, of the desired signal is also visible in Fig. 10.

G. Important Remarks

As shown in Sec. III-F, DAIM suppresses CCI significantly as v increases. The optimum v is dependent on many system parameters such as B_w , f_c and environmental and topological parameters such as θ , ω , and K . Hence, v should be carefully selected, and be able to be adapted to the environment. From

Fig. 6 and also in general, a rotation velocity that achieves $f_D = 2B_w$ (which is about $v = 2\lambda_c B_w \sin \theta$) is a reasonable value for v . It is equivalent to $v = 58$ m/s for $B_w = 5$ KHz, and $v = 23$ m/s for $B_w = 2$ KHz. From geometry of the drum antenna, the angular rotation speed can be obtained as:

$$s_r = \frac{30v}{\pi R} = \frac{60CB_w}{\pi f_c R} \text{ RPM}, \quad (26)$$

where s_r is the angular rotation speed in rounds per minute (RPM), which is about 1100 RPM for $B_w = 2$ KHz, $R = 20$ cm and $f_c = 60$ GHz. The equation, (26) also shows that R and s_r can be traded-off for one another. Furthermore, it appears that DAIM can only be applied practically for mmWave frequencies with B_w in the order of KHz and ultra-narrowband (UNB) communication systems with sub-GHz carrier frequencies with B_w in the order of Hz. Other scenarios may require extremely high rotation velocities which may not be practically realizable with today's technologies. Otherwise, the results presented in this paper theoretically hold for any system that satisfies the assumptions considered in this paper.

In wireless communication, all the multi-path signals contribute to the receive signal power. As rotation speed increases some desired multi-path signals that give rise to excessive Doppler shift could also (while, of course, suppressing majority of interfering multi-path signals) be suppressed out by the low pass filter (See Fig. 4-(b) and (c)). It is important to note herein that, in the proper and advanced design of DAWC systems, the choice of the rotating speed should strike an effective balance between suppressing the interfering multi-paths and the desired multi-paths.

IV. FURTHER REMARKS

A. Multi-Antenna Configurations

The DAWC systems can also be extended to accommodate multiple antennas and users as shown in Fig. 11, where a possible configuration for multi-antenna Doppler assisted system for single-user communication is shown in Fig. 11-(a). Extending (13) to a dual-antenna configuration (merely for simplicity, but readily extends to more than two antenna cases) give rise to following base-band analogue equations:

$$r_1(t) = r'_{S1}(t) + n'_1(t), \quad (27a)$$

$$r_2(t) = r'_{S2}(t) + n'_2(t). \quad (27b)$$

Note that (27) applies after low-pass filtering, and hence $r'_{S_i}(t) = h'_{S_i}(t)b_S(t)$ for $i = 1, 2$. Note herein that $h'_{S_i}(t) \neq h_{S_i}(t)$ due to Doppler effect and subsequent low-pass filtering. As shown in Fig. 12, the canisters are stacked vertically, and hence both elevation and the azimuth of the incoming rays are considered in this simulation. Consequently,⁶

$$h_{S_i}(t) = \sum_{n=0}^{N_S} \alpha_n^S e^{j2\pi f_n^S t - j\psi_n^S + j(i-1)d \cos \phi_n^S}, \quad (28)$$

⁶It is assumed herein that unit wave vector of the n th desired wave front is given by $\sin \phi_n^S \mathbf{i} + \sin \beta_n^S \mathbf{j} + \cos \phi_n^S \mathbf{k}$, and antenna velocity vector of the i th drum antenna is $v_i \mathbf{i}$. See Fig. 12 for an illustration.

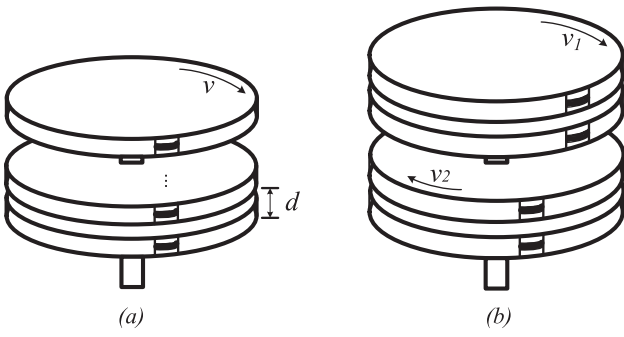


Fig. 11. (a) multi-antenna system for single-user communication and (b) multi-antenna system for multi-user configuration, where a setting for two-user system is shown to reduce the clutter.

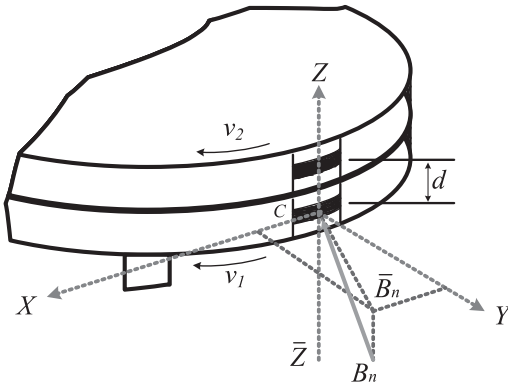


Fig. 12. An enlarged multi-antenna part-canister system that shows the azimuth and elevation of incoming rays. Only a single desired incoming ray, $B_n C \bar{Z} = \phi_n^S$ and $\bar{B}_n C Y = \beta_n^S$, is shown to reduce the clutter, where $B_n C \bar{Z} = \phi_n^S$ and $\bar{B}_n C Y = \beta_n^S$.

546 where $f_n^S = v_i \frac{f_c}{c} \sin \phi_n^S \sin \beta_n^S$, and $\psi_n^S \sim \mathcal{U}(0, 2\pi)$. Note
 547 that β_n^S and ϕ_n^S respectively are azimuth and elevation of the
 548 n th incoming ray measured in anti-clockwise direction with
 549 respect to CY and $C\bar{Z}$ axis respectively (see Fig. 12). Also,
 550 $\beta_n^S \sim \mathcal{U}(-\omega/2, \omega/2)$, and $\phi_n^S \sim \mathcal{U}(\pi/2 - \omega/2, \pi/2 + \omega/2)$,
 551 where it is assumed that both azimuth and elevation spread
 552 are the same. Note that 0th path denotes the dominant multi-
 553 path, and hence, $\beta_0^S = 0$, and it is also assumed that $\phi_0^S =$
 554 1.39626 which is 80° degrees and $d = 6\lambda_c = 3\text{cm}$. Similar
 555 fashion, $h_{Ii}(t)$ can also be obtained with the notable exception
 556 of $f_n^I = v_i \frac{f_c}{c} \sin \phi_n^I \sin(\theta + \beta_n^I)$. The ideal maximum ratio
 557 combining (MRC) can be achieved by:

$$\hat{r}(t) = (\mathbf{h}'_S(t))^H \mathbf{r}(t), \quad (29)$$

559 where $\hat{r}(t)$ is the combiner output and $(\mathbf{h}'_S(t))^H$ is the
 560 Hermitian conjugate of $\mathbf{h}'_S(t)$, $\mathbf{h}'_S(t) = \{h'_{S1}(t) h'_{S2}(t)\}^T$
 561 and also $\mathbf{r}(t) = \{r_1(t) r_2(t)\}^T$. However, often $h'_{Si}(t)$
 562 cannot be estimated exactly, and one reasonable remedy is to
 563 use \hat{h}_{Si} which is also used for data detection in (16), and note
 564 that the multi-antenna DAIM simulations in this section also
 565 employ \hat{h}_{Si} . Fig. 13 shows SIR_A performance after DAIM
 566 processing and combining, where T is the number of drum
 567 antennas configured as shown in Fig. 11-(a). It is clear that
 568 SIR_A improves significantly as T increases, and interestingly,
 569 one can manipulate the number of antennas, T , and the rotation
 570 speed, v , in order to achieve a certain SIR_A performance.

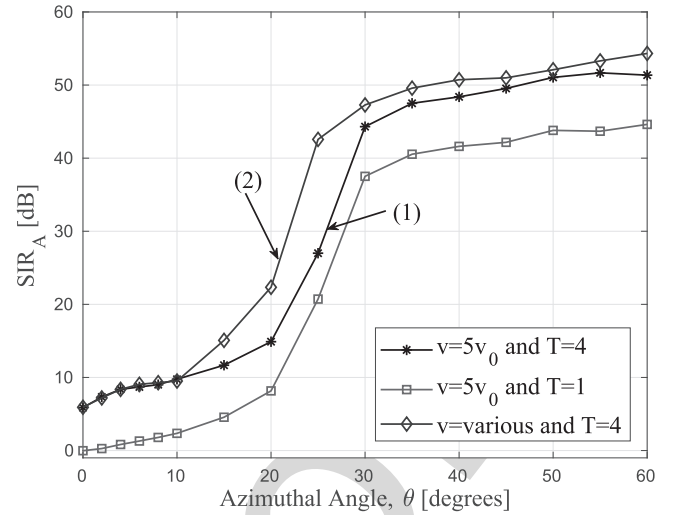


Fig. 13. SIR_A performance of multi-antenna DAIM for $\text{SIR} = 0$ dB, where $K = 10$ dB, $N = 20$, and $\omega = 10^\circ$. Note that $v_0 = \lambda_c B_w$.

It is anticipated that better channel estimation techniques shall
 571 increase SIR_A further. Note that all the drum antennas rotate
 572 at the same speed ($v = 5v_0$) for curve (1) in Fig. 13 which is
 573 not a necessary requirement.
 574

The Fig. 13 also shows (see curve (2)) the SIR_A perform-
 575 ance of a multi-antenna DAIM system with drums being
 576 rotated at different speeds of $v = 3v_0, 4v_0, 5v_0$, and $6v_0$. Let
 577 this speed profile be denoted as $\mathcal{SP}_2 = \{3v_0, 4v_0, 5v_0, 6v_0\}$.
 578 It is clear that SIR_A performance is always better than or the
 579 same as the case with drums being rotated at the same speed
 580 (i.e. a speed profile of $\mathcal{SP}_1 = \{v = 5v_0, 5v_0, 5v_0, 5v_0\}$). The
 581 energy required to rotate a single drum is proportional to the
 582 square of its angular velocity⁷ and in turn to the square of v .
 583 Hence, total energy, E_T required to rotate drum antennas in
 584 different profiles are:
 585

$$E_T \propto \begin{cases} 100v_0^2 & \mathcal{SP}_1, \\ 86v_0^2 & \mathcal{SP}_2, \end{cases} \quad (30)$$

and from kinetic energy efficiency perspective, \mathcal{SP}_2 is prefer-
 587 able as it is 14% more energy efficient than \mathcal{SP}_1 .
 588

B. Future Research

589 Even though the canister opening is directed to the direction
 590 of dominant scatters of the desired user, some non-dominant
 591 scatters can still induce fluctuations in the desired channel.
 592 Though these fluctuations can be harnessed to obtain some
 593 diversity gain as discussed in Sec. III-F, some deployments
 594 might prefer minimal channel fluctuations. Very closely and
 595 vertically placed oppositely rotating drum antennas could be
 596 used to reduce Doppler induced channel fluctuations. Note
 597 that this approach may not reduce Doppler shift in all fading
 598 conditions, and more research is required to understand the
 599 full potential of this approach. Furthermore, as shown in
 600 Fig. 11-(b), multi-antenna configuration can also be used for
 601 multi-user communication.
 602

⁷This is due to the fact that kinetic energy required to rotate a rigid body
 at certain angular velocity is $0.5I\omega^2$, where I is the moment of inertia and
 the angular velocity respectively.

The current paper discusses the basic operation of DAWC, and demonstrates the feasibility of it for CCI mitigation. We have herein used standard modulation techniques, channel estimation techniques, pulse shaping and filtering methods just to demonstrate the feasibility of the proposed system. It is expected that more tailored data modulation techniques [20], pulse shaping/filtering and also channel estimation techniques [21], [22] will increase the robustness and the performance of the proposed scheme.

It is also important to study other use cases of DAIM. In this paper, we have assumed that the interference occurs from a single interferer. If interference occurs from unknown number of interferers from unknown locations spread over a large azimuth, the state-of-the-art techniques like MIMO can be very ineffective due to their high reliance on CSI. However, DAIM, in these type of extremely hostile environments could be very effective.

V. CONCLUSIONS

The current paper has introduced, and studied a new class of systems termed as Doppler assisted wireless communication (DAWC in short). The proposed class of systems employs rotating drum antennas, and exploits Doppler effect, kinetic energy, and the topological information of wireless networks for CCI mitigation. This paper includes a detailed simulation study that models several important system and environmental parameters. The results presented herein show that difficult CCI—in the sense that it is statistically no more or less strong to the desired signal, and often poorly handled by existing interference mitigation techniques—can successfully be mitigated by the proposed system. This paper has also discussed several important phenomena occurred in DAWC systems such as Doppler gain along with advantages and challenges of DAWC.

REFERENCES

- [1] A. Osseiran *et al.*, "Scenarios for 5G mobile and wireless communications: The vision of the METIS project," *IEEE Commun. Mag.*, vol. 52, no. 5, pp. 26–35, May 2014.
- [2] J. Zander, "Distributed cochannel interference control in cellular radio systems," *IEEE Trans. Veh. Technol.*, vol. 41, no. 3, pp. 305–311, Aug. 1992.
- [3] M. Park and P. Gopalakrishnan, "Analysis on spatial reuse, interference, and MAC layer interference mitigation schemes in 60 GHz wireless networks," in *Proc. IEEE Int. Conf. Ultra-Wideband*, Vancouver, BC, Canada, Sep. 2009, pp. 1–5.
- [4] Z. Chen, C. Wang, X. Hong, J. Thompson, S. A. Vorobyov, and D. Yuan, "Cross-layer interference mitigation for cognitive radio MIMO systems," in *Proc. IEEE ICC*, Kyoto, Japan, Jun. 2011, pp. 1–6.
- [5] Z. Ding *et al.*, "Application of non-orthogonal multiple access in LTE and 5G networks," *IEEE Commun. Mag.*, vol. 55, no. 2, pp. 185–191, Feb. 2017.
- [6] Y. Saito *et al.*, "Non-orthogonal multiple access (NOMA) for cellular future radio access," in *Proc. IEEE VTC-Spring*, Dresden, Germany, Jun. 2013, pp. 1–5.
- [7] P. Marsch, M. Grieger, and G. Fettweis, "Large scale field trial results on different uplink coordinated multi-point (CoMP) concepts in an urban environment," in *Proc. IEEE WCNC*, Cancun, Mexico, Mar. 2011, pp. 1858–1863.
- [8] O. El Ayach, A. Lozano, and R. W. Heath, Jr., "On the overhead of interference alignment: Training, feedback, and cooperation," *IEEE Trans. Wireless Commun.*, vol. 11, no. 11, pp. 4192–4203, Nov. 2012.
- [9] L. C. Godara, "Application of antenna arrays to mobile communications. II. Beam-forming and direction-of-arrival considerations," *Proc. IEEE*, vol. 85, no. 8, pp. 1195–1245, Aug. 1997.

- [10] S. Haykin, "Cognitive radio: Brain-empowered wireless communications," *IEEE J. Sel. Areas Commun.*, vol. 23, no. 2, pp. 201–220, Feb. 2005.
- [11] D. A. Basnayaka *et al.*, "Doppler effect assisted interference mitigation for wireless communication," in *Proc. IEEE Global Commun. Conf.*, Abu Dhabi, UAE, 2018.
- [12] L. Lu *et al.*, "An overview of massive MIMO: Benefits and challenges," *IEEE J. Sel. Topics Signal Process.*, vol. 8, no. 5, pp. 742–758, Oct. 2014.
- [13] A. Paulraj *et al.*, "Introduction to Space-Time Wireless Communications," Cambridge, U.K.: Cambridge Univ. Press, 2003.
- [14] T. L. Koch and U. Koren, "Semiconductor lasers for coherent optical fiber communications," *J. Lightw. Technol.*, vol. 8, no. 3, pp. 274–293, Mar. 1990.
- [15] M. Gregory *et al.*, "TESAT laser communication terminal performance results on 5.6 Gbit coherent inter satellite and satellite to ground links," in *Proc. Int. Conf. Space Opt.*, Rhodes, Greece, Oct. 2010.
- [16] A. Goldsmith, *Wireless Communications*, Cambridge, U.K.: Cambridge Univ. Press, 2005.
- [17] G. L. Stüber, *Principles of Mobile Communication*, 2nd ed. Norwell, MA, USA: Kluwer, 2002.
- [18] D. A. Basnayaka, P. J. Smith, and P. A. Martin, "Performance analysis of macrodiversity MIMO systems with MMSE and ZF receivers in flat rayleigh fading," *IEEE Trans. Wireless Commun.*, vol. 12, no. 5, pp. 2240–2251, May 2013.
- [19] S. S. Haykin, *Adaptive Filter Theory*, 5th ed. London, U.K.: Pearson, 2013.
- [20] T. Dean, M. Chowdhury, and A. Goldsmith, "A new modulation technique for Doppler compensation in frequency-dispersive channels," in *Proc. IEEE PIMRC*, Montreal, QC, Canada, Oct. 2017, pp. 1–7.
- [21] P. Stoica and Y. Wang, *Spectral Analysis of Signals*, 1st ed. Upper Saddle River, NJ, USA: Prentice-Hall, 2005.
- [22] L. Zhao, G. Geraci, T. Yang, D. W. K. Ng, and J. Yuan, "A tone-based AoA estimation and multiuser precoding for millimeter wave massive MIMO," *IEEE Trans. Commun.*, vol. 65, no. 12, pp. 5209–5225, Dec. 2017.



Dushyantha A. Basnayaka (S'11–M'12–SM'18) received the B.Sc. Eng. degree (Hons.) and the Ph.D. degree in electrical and electronics engineering in 2006 and 2012, respectively. He is currently with the Institute for Digital Communications, The University of Edinburgh, U.K. His research interests include MIMO, physical layer aspects of IoT, and 5G. He holds two patents (one granted and one pending) in coordinated multi-point (CoMP) and IoT. He is a member of IEEE Communication Theory Society. He was a recipient of the University of Canterbury International Doctoral Scholarship from 2009 to 2012 and the Best Paper Award at the IEEE Vehicular Technology Conference (VTC-Spring) in 2015.



Tharmalingam Ratnarajah (A'96–M'05–SM'05) was the Head of the Institute for Digital Communications (2016–2018). He is currently with the Institute for Digital Communications, The University of Edinburgh, Edinburgh, U.K., as a Professor in digital communications and signal processing. His research interests include signal processing and information theoretic aspects of 5G and beyond wireless networks, full-duplex radio, mmWave communications, random matrices theory, interference alignment, statistical and array signal processing, and quantum information theory. He has published over 350 publications in these areas and holds four U.S. patents. He has raised over 15M € EU funding for numerous projects in many areas of wireless communication. He is a member of the American Mathematical Society and Information Theory Society and a fellow of the Higher Education Academy (FHEA). He was the Technical Co-Chair of the 17th IEEE International Workshop on Signal Processing Advances in Wireless Communications, Edinburgh, U.K., in 2016. He was an Associate Editor of the IEEE TRANSACTIONS ON SIGNAL PROCESSING (2015–2017).